https://doi.org/10.5194/egusphere-2026-5275
Preprint. Discussion started: 12 November 2026
© Author(s) 2026. CC BY 4.0 License.

Extreme Surface Incident Solar Radiation over China: Observations, ERA5, and MERRA-2

Yanyi He[1*]

[1] School of Geography and Planning, Sun Yat-sen University, 510006 Guangzhou, China

*Corresponding Author: Yanyi He (heyy99@mail.sysu.edu.cn)

https://doi.org/10.5194/egusphere-2026-5275
Preprint. Discussion started: 12 November 2026
© Author(s) 2026. CC BY 4.0 License.



Abstract

Daily surface incident solar radiation (R_s) from reanalysis products is widely used to assess the reliability, stability, and intermittency of photovoltaic power generation and other applications, owing to their full spatiotemporal coverage and physical consistency. However, whether reanalyses faithfully represent the characteristics of extreme R_s remains insufficiently evaluated. To address this, we assessed the performance of two major reanalysis products, ERA5 and MERRA-2, in simulating mean and extreme R_s across China during 1961–2016 with the help of precious ground-based observations of daily R_s. Observational analysis of mean R_s shows pronounced solar dimming before 1994, followed by weak brightening. Extremely high R_s (R_s90p) frequency presents multidecadal variations broadly consistent with mean R_s, whereas its magnitude increases persistently from 1980 onward. Conversely, extremely low R_s (R_s10p) frequency increases steadily during 1961–2016, while its magnitude decreases until 1994 and then reverses thereafter. Although ERA5 broadly captures most segmented variations of both extremes, it underestimates by over 90% the pre-1980 decline in R_s90p frequency and the post-1994 increases in the frequencies of both extremes. MERRA-2 performs worse than ERA5, particularly in failing to reproduce the evolution of R_s90p frequency and magnitude. The attribution analysis reveals that trend biases in R_s90p are predominantly controlled by those in clear-sky R_s in reanalysis products whereas cloud- and aerosol-related processes jointly influence trend biases in R_s10p. These findings highlight the limitations of current reanalyses in simulating extreme R_s and the need to interpret cautiously their long-term trends in climate and solar energy applications.

https://doi.org/10.5194/egusphere-2026-5275
Preprint. Discussion started: 12 November 2026
© Author(s) 2026. CC BY 4.0 License.

1. Introduction

Surface incident solar radiation (R_s) is a fundamental component of the Earth's energy balance and plays a central role in regulating land-atmosphere interactions, hydrological processes, ecosystems, and the climate system (Wild, 2009; Wild, 2012; Mauritsen et al., 2025). Long-term changes in R_s have been widely documented as solar dimming and brightening, with important contributions from clouds, aerosols, and atmospheric circulation (Sanchez-Lorenzo et al., 2009; Sanchez-Lorenzo et al., 2015; Manara et al., 2016). In particular, increasing attention has been paid to extreme R_s events, since extremely high R_s events can exacerbate heat stress and drought (Horton et al., 2016; Dirmeyer et al., 2021; Guan et al., 2025; Lin et al., 2026), while extremely low R_s events can suppress photosynthesis and reduce solar power generation efficiency (Wang et al., 2024; Zheng et al., 2024). These impacts underscore the need to accurately assess the characteristics of R_s extremes for climate, ecological, and energy applications.

Reanalysis products are widely used across a broad range of fields to characterize long-term variations in R_s owing to their global coverage, temporal continuity, and physical consistency (Zhou et al., 2018; Qin et al., 2019; Tong et al., 2021; Jiang et al., 2023). Despite continuous improvements in reanalysis products, substantial uncertainties remain in their capability to reproduce observed R_s variations, including a general overestimation of multiyear mean R_s values and a limited skill in capturing long-term R_s trends (Huang et al., 2018; Babar et al., 2019; Wohland et al., 2020; He et al., 2021a). Specifically, Urraca et al. (2018) reported that the fifth-generation ECMWF atmospheric reanalysis (ERA5; Hersbach et al., 2020) exhibits a global positive bias of 4.05 $W \cdot m^{-2}$, representing a 50–75% reduction in bias relative

https://doi.org/10.5194/egusphere-2026-5275
Preprint. Discussion started: 12 November 2026
© Author(s) 2026. CC BY 4.0 License.

to ECMWF Interim Reanalysis (ERA-Interim; Dee et al., 2011) and the Modern-Era Retrospective Analysis for Research and Applications, Version 2 (MERRA-2; Gelaro et al., 2017). Feng and Wang (2019) reported that five reanalysis products, namely ERA-Interim, Japanese 55-year Reanalysis (JRA-55; Kobayashi et al., 2015), National Centers for Environmental Prediction Climate Forecast System Reanalysis (NCEP-CFSR; Saha et al., 2010), Modern-Era Retrospective Analysis for Research and Application (MERRA; Rienecker et al., 2011), and MERRA-2, overestimated the multiyear mean R_s over China by 24.10–40.00 $W \cdot m^{-2}$ relative to estimates derived from sunshine duration during 1980–2014, with substantial biases in R_s trends ranging from approximately -20 to 20 $W \cdot m^{-2} \cdot decade^{-1}$. He et al. (2021a) examined the latest reanalysis and revealed that the overestimation of multiyear mean of R_s over China during 1979–2014 is reduced from 15.88 $W \cdot m^{-2}$ in ERA-Interim to 10.07 $W \cdot m^{-2}$ in ERA5, with the declining R_s trend in ERA5 being closer to observations. Du et al. (2022) showed that MERRA-2 overestimates hourly and daily mean R_s over China by 69.35 $W \cdot m^{-2}$ and 27.54 $W \cdot m^{-2}$, respectively. In addition, Wohland et al. (2020) evaluated four centennial reanalyses (20CRv2c, 20CRv3, ERA20C, and CERA20C) and one free-running model simulation (ERA20CM) over Europe, finding that only CERA20C broadly reproduced the observed dimming (1949–1979) and brightening (1979–2009) patterns in R_s. These studies also suggest that biases in reanalysis R_s are closely linked to deficiencies in the representation of clouds and aerosols, particularly cloud fraction, cloud optical properties, and aerosol radiative effects. Differences in the treatment of these processes, together with variations in observational data assimilation and radiation parameterizations, may partly explain the contrasting performance among reanalysis products.

https://doi.org/10.5194/egusphere-2026-5275
Preprint. Discussion started: 12 November 2026
© Author(s) 2026. CC BY 4.0 License.

Previous studies have also shown that separating all-sky and clear-sky R_s provides a useful framework for diagnosing the relative roles of cloud-related and clear-sky processes in observed dimming and brightening (Manara et al., 2016). However, uncertainties in these processes may also affect the simulated frequency, magnitude, and long-term trends of extreme R_s events, yet their implications for extreme R_s remain poorly understood. In particular, it remains unclear how reliably reanalysis products reproduce extreme R_s characteristics and to what extent biases in cloud cover and clear-sky R_s are associated with discrepancies in these extremes. Addressing these questions is particularly important given the widespread use of reanalysis products, especially ERA5 and MEERA-2, as substitutes for observations in climate and renewable energy applications, including assessments of photovoltaic power generation reliability and compound heat-drought extremes (Horton et al., 2016; Wang et al., 2024; Zheng et al., 2024).

With the help of precious long-term ground-based observations of daily R_s and auxiliary meteorological variables from 1961 to 2016 over China, this study provides a quantitative examination of the performance of ERA5 and MERRA-2 in simulating extreme R_s, further links biases in extreme R_s to cloud-related and clear-sky radiative errors and quantify their contribution to trend biases of extreme R_s. By comparison with observations, this study aims to provide a benchmark for the reliability of reanalysis products in simulating extreme R_s, thereby informing climate change diagnostics, extreme-event risk assessments, solar energy applications.

2. Data and Methods

2.1 Ground-based observations

https://doi.org/10.5194/egusphere-2026-5275
Preprint. Discussion started: 12 November 2026
© Author(s) 2026. CC BY 4.0 License.

The China Meteorological Administration (CMA; https://data.cma.cn) maintains a nationwide network of ground-based meteorological stations with R_s observations dating back to 1957. Although these observations continue to the present, the historical R_s dataset, previously available through the CMA data platform, is no longer publicly accessible. This study uses daily R_s data through 2016, previously acquired through academic collaboration. The data were subjected to quality-control procedures, including outlier identification, internal consistency check, temporal consistency checks, and artificial checks, following the established quality-control practices (Zhou et al., 2018). To ensure sufficient data completeness, stations were required to have at least 80% of valid daily observations within each calendar month, each calendar year, and the entire period of 1961–2016. A total of 55 stations met these criteria and were retained for subsequent homogenization and analysis (Fig. 1).

Some issues in daily R_s records have been reported to remain, including instrument aging and sensitivity drift prior to 1990 and instrument replacement during 1990–1993, which could result in spurious dramatic R_s trends in China (Tang et al., 2011; Wang et al., 2015; Wang and Wild, 2016; He and Wang, 2020). Based on the established experience from Zhou et al. (2021) and He et al. (2025), the homogenization was performed by first constructing a reference R_s series derived from sunshine duration and then deriving the difference series between the raw and reference R_s series by regression (He et al., 2025). The use of the difference series can effectively filter out most background climate variations, preventing true climate signals from confounding the detection of non-climatic breakpoints, which has been practically demonstrated to greatly enhance the signal-to-noise ratio and robustly isolate spurious breakpoints (Wang et al., 2015; Zhou et al., 2021; He et al., 2025). Breakpoints in the difference

https://doi.org/10.5194/egusphere-2026-5275
Preprint. Discussion started: 12 November 2026
© Author(s) 2026. CC BY 4.0 License.

series were identified in the mean using the PMFred method, a Penalized Maximal F-test (Wang, 2008; Wang and Feng, 2013) and in the variance using the K-S test, an improved Kolmogorov-Smirnov test (Wang et al., 2010; Zhou et al., 2021). The detected breakpoints in both the mean and variance were subsequently corrected using quantile-matching adjustment to produce the final homogenized R_s dataset. Specifically, statistically significant breakpoints ($p < 0.05$) were adjusted using a quantile-matching procedure, in which each segment was aligned to the most recent reference segment using five years of observations before and after each breakpoint (Wang et al., 2010; Zhou et al., 2021). Further methodological details are provided in He et al. (2025).

Daily clear-sky surface incident solar radiation (R_c) was obtained from He et al. (2022), where it's calculated by equation (1) based on local geographical and meteorological conditions:

$$R_c = \int (\tau_{c_dir} + \tau_{c_dif}) \times I_0 dt \quad (1)$$

where τ_{c_dir} and τ_{c_dif} represent the direct and diffuse radiation transmittance under clear skies, respectively; and I_0 is the solar irradiance at the top of the atmosphere. They were calculated using a broad radiative transfer model developed by Yang et al. (2001), based on meteorological data (including air temperature, surface pressure, and relative humidity) from ground-based stations, turbidity coefficient calculated by Hess et al. (1998), and total column ozone data from Yang et al. (2006) using Nimbus-7 and Earth Probe Total Ozone Mapping Spectrometer (TOMS) observations (Mcpeters et al., 1996; Mcpeters et al., 1998) provided by the National Aeronautics and Space Administration Goddard Space Flight Center Ozone Processing Team. R_c served here as a diagnostic indicator of clear-sky atmospheric transmissivity rather than as an independent observational benchmark.

https://doi.org/10.5194/egusphere-2026-5275
Preprint. Discussion started: 12 November 2026
© Author(s) 2026. CC BY 4.0 License.

Given that the available cloud cover records terminate in 2013 and the temporal overlap between ERA5 and MERRA-2 begins in 1980, the subsequent attribution analysis is constrained to 1980–2013 to ensure data consistency and inter-comparability. R_c and TCC are temporally aligned with daily R_s observations at each station, and all reanalysis data described below are then matched to the corresponding observations to ensure consistency in missing data for subsequent analysis.

2.2 Reanalysis products

ERA5 (Hersbach et al., 2023) is the fifth-generation global atmospheric reanalysis developed by the European Centre for Medium-Range Weather Forecasts (ECMWF) as the successor to ERA-Interim, incorporating significant advances in the ECMWF Integrated Forecast System (IFS) and the availability of assimilated observations (Hersbach and Dee, 2016; Hersbach et al., 2019). ERA5 is generated by combining the IFS model (CY41R2) with an advanced 4D-Var assimilation system, which ingests a wide range of *in-situ* and satellite observations to produce a physically consistent reconstruction of the atmosphere (Hersbach and Dee, 2016). Compared with earlier reanalysis products, ERA5 offers substantially higher spatial (~31 km) and temporal (hourly) resolutions and exhibits improved performance across key atmospheric variables (Hersbach et al., 2019). In particular, its simulation of R_s has been markedly enhanced through the adoption of the Rapid Radiative Transfer Model shortwave scheme and improved representations of clouds (He et al., 2021a).

MERRA-2 is NASA's second-generation global atmospheric reanalysis, designed to succeed the original MERRA (Gelaro et al., 2017). It is produced using an updated version of the Goddard Earth Observing System model with a 3D-Var assimilation system, at a native

https://doi.org/10.5194/egusphere-2026-5275
Preprint. Discussion started: 12 November 2026
© Author(s) 2026. CC BY 4.0 License.

horizontal resolution of about 0.5° × 0.625° (~50 km) and with an hourly temporal resolution. It should be noted that MERRA-2 is the first long-term, global reanalysis to consistently incorporate dynamic aerosol information. This enables MERRA-2 to potentially provide an improved and physically consistent representation of atmospheric composition, hydrologic cycle, and key surface variables such as R_s (Gelaro et al., 2017; Feng and Wang, 2019), making MERRA-2 a critical dataset for climate research and other applications. Due to the lack of MERRA-2 data prior to 1980, the evaluation involving MERRA-2 is limited to the period 1980–2016.

To align the datasets, observational stations were spatially matched to the nearest reanalysis grid cells based on their geographic coordinates. We acknowledge that observational measurements reflect local point-scale conditions whereas reanalysis products represent spatial averages over grid cells, showing some representativeness mismatch, particularly in regions with complex terrain (Hofstra et al., 2009; Zhou et al., 2018). However, it's worth noting that the layout and selection of China's radiation stations strictly adhere to national meteorological standards (Wang et al., 2015), ensuring exceptional openness of the surrounding environment and enhancing the station's spatial representativeness, thereby minimizing potential scale-mismatch biases compared to these high-resolution of reanalysis products. Furthermore, station-based evaluation remains a widely used approach for assessing reanalysis performance due to the reliability and long-term continuity of ground measurements (Decker et al., 2012; Wang and Zeng, 2012; Zhou et al., 2017).

2.3 Methods

Following the approach for extreme temperature or precipitation indices defined by the

https://doi.org/10.5194/egusphere-2026-5275
Preprint. Discussion started: 12 November 2026
© Author(s) 2026. CC BY 4.0 License.

Expert Team on Climate Change Detection and Indices (ETCCDI; http://etccdi.pacificclimate.org/list_27_indices.shtml), daily R_s values below the 10th percentile or above the 90th were defined as extremely low (R_s10p) and high R_s (R_s90p), respectively. The 10th or 90th percentiles for each calendar day were computed over a 7-day centered window for the respective analysis period. For instance, the 10th percentile on July 1 was calculated from 392 observations of R_s, representing 7 days (June 28 to July 4) × 56 years (1961 to 2016). Based on the established community practices (Li et al., 2025; He et al., 2026), a 7-day centered window was used to compute daily percentiles to ensure sufficient samples for each percentile calculation. Sensitivity analyses confirm that alternative window sizes (e.g., 5- or 9-day) do not change the core findings of this study. The frequency (unit: days) of R_s10p or R_s90p was computed as annual count of days on which daily R_s values were below the 10th percentile or above the 90th. To account for the potential impact of missing data records, the frequency was further normalized by scaling the annual count of days with available records to 366 for leap years or 365 for the other years. The magnitude (unit: W·m^{-2}) was calculated as mean daily R_s value on those days classified as R_s10p or R_s90p.

To illustrate the impacts of these observational inhomogeneities, we made trend comparisons between raw and homogenized observations at 55 stations across China during 1961–2016, including annual mean R_s anomalies (Fig. S1) and the frequency and magnitude of extremely high (R_s90p) and low (R_s10p) radiation (Figs. S1-S2 and Table 1). Results show that the homogenization addresses both abrupt discontinuities associated with instrument replacement during 1990–1993 and gradual biases caused by instrumental sensitivity drift (Fig. S1), which is consistent with the R_s adjustment reported by Wang et al. (2015) based on

https://doi.org/10.5194/egusphere-2026-5275
Preprint. Discussion started: 12 November 2026
© Author(s) 2026. CC BY 4.0 License.

homogenized monthly observations, providing additional support for the reliability of homogenization in this study. More importantly, these inhomogeneity issues can be eliminated substantially in the assessment of extreme R_s. For example, during 1994–2016, the frequency of R_s10p exhibited a significant increasing trend of 1.92 days·decade^{-1} in the raw observations, whereas the homogenized observations showed a statistically insignificant decreasing trend of -0.84 days·decade^{-1} (Fig. S2; Table S1). This reversal demonstrates that observational inhomogeneities can introduce spurious trends in extreme R_s, underscoring the necessity of homogenization for reliable assessments of long-term solar radiation variations.

To evaluate performance of reanalysis products in capturing R_s10p and R_s90p, six metrics (Equations 2-7) were employed: accuracy, precision, specificity, false alarm rate, hit rate, and miss rate (Wilks, 2011). Let P and N denote positive (i.e., extreme R_s) and negative (non-extreme R_s) samples, respectively. Reanalysis simulations were categorized as follows: true positives (TP), positive samples correctly simulated as positive; false negatives (FN), positive samples incorrectly simulated as negative; false positives (FP), negative samples incorrectly simulated as positive; and true negatives (TN), negative samples correctly simulated as negative.

$$\text{Accuracy} = \frac{TP+TN}{TP+TN+FP+FN} \quad (2)$$

$$\text{Precision} = \frac{TP}{TP+FP} \quad (3)$$

$$\text{Specificity} = \frac{TN}{TN+FP} \quad (4)$$

$$\text{False Alarm Rate} = \frac{FP}{FP+TN} \quad (5)$$

$$\text{Hit Rate} = \frac{TP}{TP+FN} \quad (6)$$

$$\text{Miss Rate} = \frac{FN}{TP+FN} \quad (7)$$

https://doi.org/10.5194/egusphere-2026-5275
Preprint. Discussion started: 12 November 2026
© Author(s) 2026. CC BY 4.0 License.

where accuracy measures the overall proportion of correctly simulated samples by reanalysis products; precision quantifies the reliability of correctly simulated extreme R_s; specificity represents the ability to correctly simulate non-extreme R_s; false alarm rate measures the fraction of non-extreme R_s incorrectly simulated as extreme R_s; hit rate indicates the ability to reproduce extreme R_s; and miss rate represents the fraction of extreme R_s that are not simulated. Higher values of accuracy, precision, specificity, and hit rate indicate better performances of reanalysis products, whereas higher values of false alarm rate and miss rate indicate poorer performances (Wilks, 2011).

To explore the relationships between reanalysis biases in extreme R_s and the associated climatic factors, namely TCC and R_c, we conducted Pearson correlation analyses to assess their spatial correspondence. The biases were computed as reanalyses minus observations for extreme R_s days identified separately within each dataset, which were used to measure simulation errors of reanalysis products compared to observations. We further performed partial correlation analysis on the annual bias time series to examine the temporal associations between extreme R_s biases and each climatic driver while statistically controlling for the other:

$$\rho_{(x,y)|z} = \frac{r_{x,y} - r_{x,z}r_{y,z}}{\sqrt{(1-r_{x,z}^2)(1-r_{y,z}^2)}} \quad (8)$$

where $\rho_{(x,y)|z}$ is the partial correlation coefficient between x and y by controlling z; x represents the standardized R_s10p or R_s90p biases; y and z can be the standardized TCC or R_c biases; r is their Pearson correlation coefficient.

Trends were estimated by applying linear regression to annual extreme R_s series and their significance levels were evaluated by a two-tailed Student's t test. To quantify the relative contributions of biases in climatic drivers to the trend biases in extreme R_s, we employed

https://doi.org/10.5194/egusphere-2026-5275
Preprint. Discussion started: 12 November 2026
© Author(s) 2026. CC BY 4.0 License.

multiple linear regression:

$$Y = \sum \beta_i X_i + c + \varepsilon \quad (9)$$

where Y is the standardized bias in R_s10p or R_s90p between reanalysis and observations, and X_i is the standardized bias in the i-th climatic driver, including TCC and R_c. The coefficient β_i is the partial regression coefficient of i-th climatic driver, while c and ε are the intercept and residual, respectively.

The relative contribution of each climatic driver to the modeled trend bias in extreme R_s was calculated as:

$$C_i = \frac{|Tr_i \times \beta_i|}{\sum |Tr_i \times \beta_i|} \times 100\% \quad (10)$$

where C_i is the relative contribution (%) of i-th climatic driver (i.e., TCC or R_c), and Tr_i is the linear trend in the standardized bias of the i-th climatic driver. The absolute values were used to quantify the relative magnitude of each driver's contribution, irrespective of its direction.

Since ERA5 incorporates only climatological aerosol inputs instead of assimilating instantaneous data, the biases in simulated R_c were used as a proxy to represent potential influence of aerosol-related simulation difference in the subsequent analysis. Based on previous studies (He et al., 2021a; Wild et al., 2026) and available periods of reanalysis products, extreme R_s were investigated for the global dimming (1961–1979 and 1980–1993) and brightening (1994–2016) phases at temporal (climatology and trend) and spatial scales.

3. Mean R_s in observations and reanalyses

Mean R_s over China shows a significant downward trend before 1993 (Fig. 2a). This decline is most pronounced from 1961 to 1979 (-4.74 $W \cdot m^{-2} \cdot decade^{-1}$, $p < 0.05$), with ~81.8% of stations experiencing dimming and 43.6% showing statistically significant trends (Fig. 2a-

https://doi.org/10.5194/egusphere-2026-5275
Preprint. Discussion started: 12 November 2026
© Author(s) 2026. CC BY 4.0 License.

2b). During 1980–1993, the decreasing trend persists (-1.31 $W \cdot m^{-2} \cdot decade^{-1}$), though it is not statistically significant at the 0.10 level (Fig. 2a and 2d). After 1994, this trend averaged in China reverses to a slight increase of 0.97 $W \cdot m^{-2} \cdot decade^{-1}$ ($p > 0.10$), occurring at 52.7% of stations with significant increases mainly concentrated in southern China and eastern coastal areas (Fig. 2a and 2g). Previous studies have also extensively documented these long-term changes in R_s, including prominent dimming and subsequent brightening periods over China (Tang et al., 2011; Wang et al., 2015; Wang and Wild, 2016; He et al., 2018; Yang et al., 2018; He and Wang, 2020; Shao et al., 2022).

ERA5 provides R_s simulations back to 1961. During 1961–1979, it fails to reproduce the pronounced nationwide decline observed in R_s, showing a significant decline only in the southeastern region (Fig. 2a and 2c). During 1980–1993, both ERA5 and MERRA-2 reproduce a decreasing R_s (Fig. 2e and 2f), with trends of -1.89 ($p < 0.05$) and -0.81 $W \cdot m^{-2} \cdot decade^{-1}$ ($p > 0.10$), respectively. During 1994–2016, ERA5 captures an increasing trend in R_s (1.30 $W \cdot m^{-2} \cdot decade^{-1}$, $p > 0.10$) that is consistent with observations (Fig. 2a and 2h), whereas MERRA-2 instead simulates a significant declining trend (-2.20 $W \cdot m^{-2} \cdot decade^{-1}$, $p < 0.05$) in China, particularly in the southern regions, failing to reproduce the observed solar brightening (Fig. 2h and 2i).

4. Extreme R_s in observations and reanalyses

Figure 3 shows that the R_s thresholds of different quantiles for each calendar day computed from observations and reanalyses. The differences in thresholds between from reanalyses and observations progressively decline with increasing R_s quantiles (Fig. 3). The differences or biases are largest at the 10% quantile and smallest at the 90% quantile, with ERA5 showing

https://doi.org/10.5194/egusphere-2026-5275
Preprint. Discussion started: 12 November 2026
© Author(s) 2026. CC BY 4.0 License.

312 closer agreement with observations than MERRA-2 (Fig. 3). The degraded performance from
313 R_s90p to R_s10p likely reflects contrasts in their dominant physical controls. R_s90p is typically
314 associated with clear-sky conditions and high atmospheric transmissivity, which are better
315 constrained in reanalysis products. Conversely, R_s10p is strongly influenced by intricate cloud–
316 aerosol–radiation interactions (Zhao et al., 2020; Teng et al., 2026), which are notoriously
317 challenging to parameterize or poorly constrained by observations, leading to larger biases in
318 reanalysis products.

319 *4.1 Climatology*

320 For R_s90p at most stations in China, the multiyear average frequency in observations is
321 higher during 1961–1979 (~55 days) than in the subsequent periods of 1980–1993 (~30 days)
322 and 1994–2016 (~24 days), whereas the multiyear average magnitude peaks during 1994–2016
323 (~266 $W \cdot m^{-2}$) (Fig. 4a, 4c, and 4f). During 1961–1979, ERA5 generally underestimates R_s90p
324 frequency at most stations of China and overestimates R_s90p magnitude in particular for
325 northwest China relative to observations (Fig. 4a-b). During 1980–1993, both ERA5 and
326 MERRA-2 display similar spatial patterns in R_s90p frequency, with higher values in southern
327 China and lower values in northern China (Fig. 4d-e), but this meridional contrast is much
328 weaker in observations (cf. Fig. 4c). In this period, MERRA-2 exhibits a more pronounced
329 overestimation of R_s90p frequency than ERA5, particularly in southeastern China (Fig. 4d and
330 4e). During 1994–2016, both reanalysis products consistently underestimate R_s90p magnitude
331 and overestimate R_s90p frequency across most regions (Fig. 4f-h). In contrast to observations
332 and ERA5, MERRA-2 shows a distinct spatial pattern in R_s90p magnitude, with higher values
333 in southern China and lower values in northern China (Fig. 4f-h).

https://doi.org/10.5194/egusphere-2026-5275
Preprint. Discussion started: 12 November 2026
© Author(s) 2026. CC BY 4.0 License.

For R_s10p in observations, its frequency pattern that lower values in the west and higher in the east before 1993 shifts to the opposite after 1994, while its magnitude consistently remains higher in the west than in the east (Fig. 5a, 5c and 5f). Both ERA5 and MERRA-2 evidently overestimate R_s10p magnitude for all three periods, particularly pronounced in western China and in MERRA-2 (Fig. 5). During 1980–1993, MERRA-2 underestimates R_s10p frequency more than ERA5 referenced to observations, particularly in southeastern China (Fig. 5c-e). During 1994–2016, ERA5 continues to underestimate R_s10p frequency, whereas MERRA-2 overestimates it in southern China.

Six metrics were adopted to quantity the overall performance of reanalysis products in capturing R_s90p and R_s10p: accuracy, precision, specificity, false alarm rate, hit rate, and miss rate. For R_s90p, ERA5 performs slightly better than MERRA-2 across most metrics, except for hit rate and miss rate (Fig. 6). This suggests a slightly more robust yet somewhat conservative representation of high R_s extremes, likely reflecting differences in cloud-radiation parameterizations and data assimilation strategies that prioritize reduced false alarms over increased detection of high R_s extremes. For R_s10p, ERA5 outperforms MERRA-2 across all six metrics, highlighting a clearer advantage in representing low R_s extremes (Fig. 6).

4.2 Long-term variations

Figure 7 shows time series of annual frequency and magnitude of R_s90p and R_s10p averaged in China from observations and reanalysis products from 1961 to 2016. Observed R_s90p frequency exhibits a pronounced decline (-18.31 days·decade^{-1}, $p < 0.05$) during 1961–1979, followed by relatively low values during the 1980s and 1990s, and a significant recovery after 1994 (6.65 days·decade^{-1}, $p < 0.05$) (Fig. 7a and Table 1). ERA5 broadly reproduces the

https://doi.org/10.5194/egusphere-2026-5275
Preprint. Discussion started: 12 November 2026
© Author(s) 2026. CC BY 4.0 License.

356 overall temporal evolution and interannual variability of R_s90p frequency but underestimates
357 the early decline by ~95% and the post-1994 increase by ~91% (Fig. 7a and Table 1). In contrast,
358 MERRA-2 fails to reproduce the recent recovery and instead exhibits a continued negative
359 trend during 1994–2016 (-6.44 days·decade^{-1}, $p < 0.05$), contrary to observations (Fig. 7a and
360 Table 1).

361 Observed R_s90p magnitude exhibits weak long-term trends, with relatively enhanced
362 variability during the 1980s and early 1990s (Fig. 7c). ERA5 broadly reproduces both
363 magnitude and interannual variability, although it slightly exaggerates the early weakening (-
364 4.78 W·m^{-2}·decade^{-1} in ERA5, $p < 0.10$ vs. -0.26 W·m^{-2}·decade^{-1} in observations, $p > 0.10$)
365 (Fig. 7c and Table 1). MERRA-2 overestimates R_s90p magnitude by approximately 20–40
366 W·m^{-2} referenced to observations during 1980–1993, but significantly underestimates the
367 observed increase (7.12 W·m^{-2}·decade^{-1} in MERRA-2, $p > 0.10$ vs. 13.35 W·m^{-2}·decade^{-1} in
368 observations, $p < 0.05$) (Fig. 7c).

369 Observed R_s10p frequency evidently shows an increasing tendency (Fig. 7b). ERA5 shows
370 high consistency with observations in terms of interannual variability (Fig. 7b). During 1980–
371 1993, ERA5 exhibits a slightly stronger increase in R_s10p frequency (5.26 days·decade^{-1}, $p <$
372 0.05) than the observed (2.79 days·decade^{-1}, $p < 0.05$); in contrast, during 1994–2016 ERA5
373 shifts to a weak negative trend (-0.84 days·decade^{-1}, $p > 0.10$), whereas observations maintain
374 a significant positive trend (1.92 days·decade^{-1}, $p < 0.05$) (Fig. 7b), indicating that ERA5
375 slightly underestimates the sustained increase in R_s10p frequency in recent decades. MERRA-
376 2 reproduces the overall upward tendency in R_s10p frequency but exhibits larger interannual
377 fluctuations and a weaker trend during the earlier period (Fig. 7b), indicating an improvement

https://doi.org/10.5194/egusphere-2026-5275
Preprint. Discussion started: 12 November 2026
© Author(s) 2026. CC BY 4.0 License.

in trend representation than ERA5 in recent decades.

For R_s10p magnitude, observations remain relatively stable, with a notable weakening (-3.70 W·m^{-2}·decade^{-1}, $p < 0.05$) during 1980–1993 (Fig. 7d). ERA5 markedly overestimates R_s10p magnitude by an average of ~26.8 W·m^{-2} referenced to observations but roughly reproduces decadal trends, including the pronounced decrease (-4.18 W·m^{-2}·decade^{-1}, $p < 0.05$) during 1980–1993 (Fig. 7d and Table 1). MERRA-2 shows a substantial bias (~56.3 W·m^{-2}) whose quantity is on the order of the observed R_s10p magnitude itself, and presents a limited skill in reproducing the R_s10p trend (Fig. 7d).

4.3 Spatial patterns of long-term variations

During 1961–1979, ERA5 generally reproduces the declining trends in R_s90p frequency across China (~60% of stations in ERA5 vs. ~76% in observations) but underestimates the degree of the declines (Fig. 8a-b). In southwestern China, ERA5 shows an opposite trend of R_s90p frequency relative to observations (Fig. 8a-b). Furthermore, ERA5 fails to reproduce both sign and degree of trends in R_s90p magnitude at most stations across China (Fig. 8a-b). For of R_s10p, ERA5 also shows limited skill in capturing spatial patterns of both frequency and magnitude trends (Fig. 9a-b).

During 1980–1993, in contrast to observations that have roughly comparable proportions of positive and negative trends in R_s90p frequency, both ERA5 (~82%) and MERRA-2 (~74%) exhibit decreasing R_s90p frequency trends at most stations across China (Fig. 8c-e). Compared with ERA5, MERRA-2 can reproduce the increasing R_s90p frequency over northeast China (Fig. 8c-e). For R_s90p magnitude, both ERA5 and MERRA-2 show weaker increasing trends than observed at the majority of stations across China, especially in southeastern China (Fig.

https://doi.org/10.5194/egusphere-2026-5275
Preprint. Discussion started: 12 November 2026
© Author(s) 2026. CC BY 4.0 License.

8c-e). For R_s10p, ~73%, ~85%, and ~60% of stations across China exhibit positive frequency trends in observations, ERA5, and MERRA-2, respectively, while ~77%, ~78%, and ~78% of stations show negative magnitude trends (Fig. 9c-e). Compared with MERRA-2, ERA5 better reproduces the spatial patterns of R_s10p frequency and magnitude trends, although it tends to overestimate the frequency increases and underestimate the magnitude declines at most stations across China (Fig. 9c-e).

During 1994–2016, MERRA-2 performs poorly in simulating R_s90p frequency, with ~92% of stations exhibiting negative trends, which is much inconsistent with observations (Fig. 8f and 8h). ERA5 reproduces the sign of the R_s90p frequency trend over southern China that is generally consistent with observations, but the degree of the trend is underestimated (Fig. 8f-g). Observations indicate an increasing frequency but decreasing magnitude in R_s90p over northeastern China (Fig. 8f), but neither reanalysis product is able to reproduce this observed change (Fig. 8g-h). For R_s10p frequency, observations show significantly increasing trends in northern China and significantly decreasing trends in southern China, whereas both ERA5 and MERRA-2 fail to capture this spatial contrast (Fig. 9f-h). For R_s10p magnitude, observations exhibit significantly increasing trends in southeastern China, while both EAR5 and MERRA-2 indicate decreasing trends, with the declining trends in MERRA-2 being statistically significant (Fig. 9f-h). In North China, R_s10p frequence increases but R_s10p magnitude decreases, suggesting an intensification in the severity of extremely low R_s, which may have serious implications for local agricultural production and photovoltaic power generation (Takahashi et al., 2019; He et al., 2021b; He et al., 2023).

5. Attribution of biases in extreme R_s

https://doi.org/10.5194/egusphere-2026-5275
Preprint. Discussion started: 12 November 2026
© Author(s) 2026. CC BY 4.0 License.

Previous studies have shown that biases in mean R_s have been revealed to primarily arise from deficiencies in cloud and aerosol simulations in reanalysis products (Feng and Wang, 2019; He et al., 2021a). However, since mean R_s integrates radiative conditions across all weather regimes, cloud- and aerosol-related processes are often difficult to disentangle. In contrast, R_s90p and R_s10p are generally governed by distinct atmospheric processes: R_s10p is associated with enhanced cloud cover and cloud optical thickness, indicating strong cloud control, whereas R_s90p is more sensitive to aerosol radiative effects. To further investigate the physical origins of reanalysis biases in R_s90p and R_s10p, we examined spatial correspondence of their climatological mean biases (section 5.1) and respective contributions of their trend biases (section 5.2) from cloud and R_c biases.

5.1 Spatial relationships between climatological biases in extreme R_s and their drivers

Figure 10 shows correlations across the 55 stations between climatological mean biases in extreme R_s and corresponding biases in TCC and R_c. For each station, climatological mean biases in R_s90p and R_s10p were calculated for extreme R_s days identified within each dataset during the study period. In ERA5, R_s10p biases exhibit a significantly negative correlation against TCC biases (r = -0.35, p = 0.01) with high sensitivity (-1.37 W·m^{-2}/%), whereas R_s90p biases show little correlation (r = -0.06, p = 0.66) (Fig. 10a). A similar relationship was found in MERRA-2 (Fig. 10b). These relationships suggest that ERA5 and MERRA-2 themselves hold a strong control of TCC biases on R_s10p biases, but little association with R_s90p biases. R_c was used as a proxy for aerosol influences on R_s. ERA5 R_s10p biases exhibit a significantly positive correlation against R_c biases (r = 0.46, p < 0.01) with high sensitivity (0.92), whereas R_s90p biases hold a weak correlation (r = 0.24, p = 0.08) (Fig. 10c). In MERRA-2, neither

https://doi.org/10.5194/egusphere-2026-5275
Preprint. Discussion started: 12 November 2026
© Author(s) 2026. CC BY 4.0 License.

444 biases in R_s10p (r = 0.19, p = 0.17) nor R_s90p (r = 0.03, p = 0.83) are significantly correlated
445 with R_c biases (Fig. 10d). In a word, ERA5 spatially link R_c biases to R_s10p biases but weakly
446 to R_s90p biases, whereas MERRA-2 shows no such associations.

447 To assess the roles of cloud and aerosol simulation errors under actual extreme R_s
448 conditions, we further examined the relationships between biases in R_s90p and R_s10p and biases
449 in TCC and R_c for extreme R_s days identified by observations (Fig. 11). In term of spatial
450 correlations, R_s10p biases in ERA5 exhibit a significant negative correlation with TCC bias (r
451 = -0.54, p < 0.05) (Fig. 11a). ERA5 holds a similar but weaker relationship between R_s90p
452 biases and TCC bias (r = -0.50, p < 0.05), with a lower sensitivity than that of R_s10p (-1.43 vs.
453 -1.79 W·m^{-2}/%) (Fig. 11a). These relationships indicate that biases in extreme R_s are largely
454 governed by errors in cloud representation, with a stronger influence on R_s10p than on R_s90p.
455 Compared with ERA5, cloud biases in MERRA-2 still exert a strong control on R_s10p biases
456 (r = -0.49, p < 0.05) with higher sensitivity (-2.19 vs. -1.79 W·m^{-2}/%), but their influence on
457 R_s90p biases is much weaker and statistically non-significant (r = -0.21, p > 0.10) (Fig. 11b).
458 In ERA5, biases in R_s90p and R_s10p show a comparably positive correlation with R_c biases (r
459 = 0.37 vs. 0.45, p < 0.01) (Fig. 11c). In MERRA-2, R_s90p biases exhibit a relatively weak but
460 significantly positive correlation with R_c biases (r = 0.29, p = 0.03), whereas R_s10p biases is
461 not correlated with R_c biases ($r \approx 0$, sensitivity ≈ 0) (Fig. 11d). This contrast indicates that R_c
462 biases are spatially associated with R_s90p biases but not with R_s10p biases.

463 *5.2 Temporal relationships between biases in extreme R_s and their drivers*

464 Figure 12 illustrates the spatial distributions of station-wise partial correlation coefficients
465 calculated from the annual time series between reanalysis biases in extreme R_s (i.e., ΔR_s90p

https://doi.org/10.5194/egusphere-2026-5275
Preprint. Discussion started: 12 November 2026
© Author(s) 2026. CC BY 4.0 License.

and ΔR_s10p) and the corresponding biases in TCC (ΔTCC) and R_c (ΔR_c). The reanalysis biases were computed as reanalyses minus observations for extreme R_s days identified separately within each dataset. For ERA5, significant negative partial correlations between ΔR_s10p and ΔTCC primarily cluster over northern China (Fig. 12a and 12i), indicating that larger positive TCC biases are generally relevant to larger negative R_s10p biases. Conversely, positive partial correlations between ΔR_s10p and ΔR_c are widespread across China, but are generally stronger in western China and weaker over the North China Plain (35°-42°N, 110°-120°E) (Fig. 12b and 12i). These pattern contrasts suggest that cloud-related errors exert a stronger influence on ΔR_s10p in northern China, whereas R_c errors become increasingly important in western regions. MERRA-2 shares a similar spatial pattern of partial correlations between ΔR_s10p and ΔTCC to that of ERA5, characterized by negative correlations over northern China (Fig. 12e and 12i). However, significant positive correlations between ΔR_s10p and ΔR_c occur across larger domain of China, including the North China Plain (Fig. 12f and 12i), suggesting a more widespread influence of R_c biases than in ERA5.

Both ERA5 and MERRA-2 clearly exhibit strong positive partial correlations between ΔR_s90p and ΔR_c across the vast majority of stations (Fig. 12d, 12h, and 12i). The correlations are generally stronger in ERA5 than in MERRA-2. In contrast, partial correlations between ΔR_s90p and ΔTCC are weak and statistically insignificant at most stations (Fig. 12c, 12g and 12i). These results indicate that biases in R_c are more closely associated with biases in R_s90p than biases in cloud cover for both reanalysis products. Similar results are present for extreme R_s days identified by observations (not shown).

5.3 Contributions of trends biases in extreme R_s from those in TCC and R_c

https://doi.org/10.5194/egusphere-2026-5275
Preprint. Discussion started: 12 November 2026
© Author(s) 2026. CC BY 4.0 License.

To further dissect the mechanisms driving the trend biases between reanalyses and observations, we decomposed trend biases in extreme R_s into contributions arising from those in TCC and R_c, which represent cloud-mediated radiative variations and clear-sky atmospheric (primarily associated with aerosol radiative effects) processes, respectively.

Figure 13 shows that the responses of trend biases in extreme R_s to their physical drivers exhibit pronounced spatial heterogeneity and strong dependence on the type of extreme R_s. For R_s10p, trend biases in extreme R_s mainly arise from the combined influence of those in TCC and R_c, but their spatial distributions show distinct regional contrasts (Fig. 13a-b and 13e-f). The contribution of trend biases in TCC to those in R_s10p is more pronounced in eastern China, where cloud variability exerts strong control on low-radiation conditions, whereas its influence is substantially weaker over northwestern arid regions and the Tibetan Plateau (Fig. 13a and 13e). In contrast, the contribution of trend biases in R_c to those in R_s10p is more widespread across the country and shows relatively higher contributions in northwestern China (Fig. 13b and 13f), suggesting that clear-sky processes, particularly aerosol-related radiative effects, play a larger role in regulating low-radiation extremes in regions with limited cloud influence.

For R_s90p, the contribution of trend biases in TCC in is generally weak, with only limited and localized effects (Fig. 13c and 13g), indicating that cloud-related errors exert only a limited influence on long-term trends of high-radiation extremes in reanalysis products. By contrast, trend biases in R_c exhibits consistently high contributions to those in R_s90p across the entire country, with a highly uniform spatial pattern (Fig. 13d and 13h), demonstrating that clear-sky atmospheric processes dominate the representation of high-radiation extremes in reanalysis products. This dominance is physically expected since high-radiation extremes typically occur

https://doi.org/10.5194/egusphere-2026-5275
Preprint. Discussion started: 12 November 2026
© Author(s) 2026. CC BY 4.0 License.

under cloud-free or nearly cloud-free conditions, making the accurate representation of clear-sky transmissivity and its long-term evolution far more critical than cloud variability.

6. Conclusions and discussion

Surface incident solar radiation (R_s) is a fundamental component of the Earth's energy balance. Its extremes exert profound impacts on a wide range of sectors including agriculture and renewable energy production. Owing to their fully spatiotemporal coverage and completely physical consistency, reanalysis products have been widely used to force various models and as surrogate observations to assess low R_s events relevant to the stability of renewable energy system. However, their ability to reproduce the climatology and long-term variations of extreme R_s remains insufficiently evaluated. To address this gap, with the help of long-term ground-based observations of daily R_s, this study assesses the performance of two widely used reanalysis products, ERA5 and MERRA-2, in representing the climatology and long-term variations in extreme R_s over China during 1961–2016, and further quantifies the contributions of trend biases in extreme R_s from those in associated drivers.

Observation-based analysis shows that R_s90p occurs more frequently during 1961–1979, whereas their magnitudes peak during 1994–2016. In contrast, R_s10p shows a persistent increase in frequency from 1961 to 2016, accompanied by declined long-term changes in magnitude. ERA5 broadly reproduces the multidecadal characteristics of both R_s90p and R_s10p, capturing their temporal evolution and spatial patterns more realistically than MERRA-2. For R_s90p, ERA5 represents overall frequency changes and interannual variability, though it slightly underestimates long-term magnitude trends and some regional contrasts, such as the post-1994 over northeastern China. MERRA-2 performs notably worse and exhibits unrealistic

https://doi.org/10.5194/egusphere-2026-5275
Preprint. Discussion started: 12 November 2026
© Author(s) 2026. CC BY 4.0 License.

long-term trends in frequency and magnitude during 1994–2016. For R_s10p, ERA5 outperforms MERRA-2 during 1980–1993, reproducing the observed interannual variability and trends in both frequency and magnitude. In contrast, during 1994–2016, MERRA-2 shows relatively better skill in simulating the national mean trends of R_s10p frequency and magnitude; however, its spatial patterns differ substantially from observations, with particularly large discrepancies over southern China. These limitations should be carefully considered when applying current reanalysis products to solar energy assessment, climate impact studies, and historical analyses and projection constrains of R_s extremes over China.

Extreme R_s, like mean R_s, is governed by in intricate cloud-aerosol-radiation processes (Ramanathan et al., 1989; Stephens, 2005; Wild, 2012; He et al., 2026; Yuan et al., 2026), yet how these processes are represented in reanalysis products remains poorly constrained. Our findings clearly demonstrate that the mechanisms underlying extreme R_s biases differ substantially, or even decouple, between extremely low and high R_s conditions. Thus, exploring extreme R_s yields a substantially cleaner framework for process-level attribution than focusing solely on mean R_s, guiding more targeted improvements for reanalysis products.

For R_s10p, both the partial correlation and trend contribution analyses indicate that cloud- and aerosol-related processes jointly influence its biases, but their relative importance varies regionally. Cloud-related biases exert a stronger influence over northern China, whereas R_c biases become increasingly important in western China, roughly consistent with previous studies (Qian et al., 2006; Qian et al., 2007). This pattern is likely attributable to the lower cloud climatology of western China, where variations in atmospheric transmissivity exert a stronger control on solar radiation than cloud variability (Stephens, 2005; Wild, 2012; Bellouin

https://doi.org/10.5194/egusphere-2026-5275
Preprint. Discussion started: 12 November 2026
© Author(s) 2026. CC BY 4.0 License.

et al., 2020). In contrast, R_s90p biases exhibit much weaker sensitivity to cloud variability and are predominantly controlled by R_c biases, as evidenced by the contribution maps of their trend biases (Fig. 13c-d and 13g-h). This reflects the reduced sensitivity of surface solar radiation to cloud variability under near cloud-free environments, where clear-sky atmospheric transmissivity becomes the dominant control (Bellouin et al., 2020).

It's worth noting that the discrepancy between observations and reanalyses is substantially larger during 1961–1979 than after 1979 (Fig. 2a). This larger mismatch may reflect the combined effects of weaker observational constraints and greater reanalysis uncertainties in the pre-satellite era (Bengtsson et al., 2004; Dee et al., 2011; Fujiwara et al., 2017; Hersbach et al., 2020). Prior to 1979, the sparse observing network and absence of satellite measurements provided limited constraints on the assimilated atmospheric state. Since cloud properties and surface radiative fluxes are generated by the forecast model rather than directly assimilated, uncertainties in the atmospheric analysis could propagate into cloud and radiative fields (He et al., 2021a), leading to biases in simulated R_s and poor representation of historical dimming during this period. Moreover, this period coincides with rapid, non-stationary changes in R_s driven by increasing anthropogenic aerosol emissions, which may be a big challenge for reanalysis systems to reproduce the observed dimming given the limited availability of realistic aerosol information and the simplified parameterization of cloud-aerosol-radiation interactions embedded within the forecast model.

Distinct from our previous reliance on R_s estimates derived from sunshine duration (He et al., 2021a; He et al., 2026), a primary advancement of this work is anchored firmly in direct historical radiometric observations. Moreover, this study extends the analysis back to 1961,

https://doi.org/10.5194/egusphere-2026-5275
Preprint. Discussion started: 12 November 2026
© Author(s) 2026. CC BY 4.0 License.

clearly demonstrating the rapid early-stage dimming and its substantial discrepancies with reanalysis products before 1979. Crucially, these pervasive discrepancies are revealed in this study to be consistently evident in both mean and extreme R_s, indicating a robust assessment of reanalysis performance.

Data availability

The ERA5 and MERRA-2 data were obtained at https://cds.climate.copernicus.eu/, and https://disc.gsfc.nasa.gov/datasets/M2T1NXRAD_5.12.4/summary?keywords=MERRA2, respectively.

Author contributions

YH conceived the study, designed the methodology, curated the observational and reanalysis datasets, performed the analysis, produced the figures, interpreted the results, and wrote and revised the manuscript.

Conflict of Interest

The author declares no conflicts of interest relevant to this study.

Financial support

This study was supported by the Starting Grant for Introduced Talents of Sun Yat-sen University (grant no. 37000-12266025), and the Guangzhou Basic and Applied Basic Research Project (grant no. 2025A04J4393).

https://doi.org/10.5194/egusphere-2026-5275
Preprint. Discussion started: 12 November 2026
© Author(s) 2026. CC BY 4.0 License.

References

Babar, B., Graversen, R., and Bostrom, T.: Solar radiation estimation at high latitudes: Assessment of the CMSAF databases, ASR and ERA5, Solar Energy, 182, 397-411, https://doi.org/10.1016/j.solener.2019.02.058, 2019.

Bellouin, N., Quaas, J., Gryspeerdt, E., Kinne, S., Stier, P., Watson-Parris, D., Boucher, O., Carslaw, K. S., Christensen, M., Daniau, A. L., Dufresne, J. L., Feingold, G., Fiedler, S., Forster, P., Gettelman, A., Haywood, J. M., Lohmann, U., Malavelle, F., Mauritsen, T., McCoy, D. T., Myhre, G., Mülmenstädt, J., Neubauer, D., Possner, A., Rugenstein, M., Sato, Y., Schulz, M., Schwartz, S. E., Sourdeval, O., Storelvmo, T., Toll, V., Winker, D., and Stevens, B.: Bounding Global Aerosol Radiative Forcing of Climate Change, Reviews of Geophysics, 58, e2019RG000660, https://doi.org/10.1029/2019RG000660, 2020.

Bengtsson, L., Hagemann, S., and Hodges, K. I.: Can climate trends be calculated from reanalysis data?, Journal of Geophysical Research: Atmospheres, 109, D11111, https://doi.org/10.1029/2004JD004536, 2004.

Decker, M., Brunke, M. A., Wang, Z., Sakaguchi, K., Zeng, X. B., and Bosilovich, M. G.: Evaluation of the reanalysis products from GSFC, NCEP, and ECMWF using flux tower observations, Journal of Climate, 25, 1916-1944, https://doi.org/10.1175/jcli-d-11-00004.1, 2012.

Dee, D. P., Uppala, S. M., Simmons, A. J., Berrisford, P., Poli, P., Kobayashi, S., Andrae, U., Balmaseda, M. A., Balsamo, G., Bauer, P., Bechtold, P., Beljaars, A. C. M., van de Berg, L., Bidlot, J., Bormann, N., Delsol, C., Dragani, R., Fuentes, M., Geer, A. J., Haimberger, L., Healy, S. B., Hersbach, H., Holm, E. V., Isaksen, L., Kallberg, P., Kohler, M., Matricardi, M., McNally, A. P., Monge-Sanz, B. M., Morcrette, J. J., Park, B. K., Peubey, C., de Rosnay, P., Tavolato, C., Thepaut, J. N., and Vitart, F.: The ERA-Interim reanalysis: Configuration and performance of the data assimilation system, Quarterly Journal of the Royal Meteorological Society, 137, 553-597, https://doi.org/10.1002/qj.828, 2011.

Dirmeyer, P. A., Balsamo, G., Blyth, E. M., Morrison, R., and Cooper, H. M.: Land-Atmosphere Interactions Exacerbated the Drought and Heatwave Over Northern Europe During Summer 2018, AGU Advances, 2, e2020AV000283, https://doi.org/10.1029/2020av000283, 2021.

Du, Y., Shi, H., Zhang, J., Xia, X., Yao, Z., Fu, D., Hu, B., and Huang, C.: Evaluation of MERRA-2 hourly surface solar radiation across China, Solar Energy, 234, 103-110, https://doi.org/10.1016/j.solener.2022.01.066, 2022.

Feng, F. and Wang, K.: Determining factors of monthly to decadal variability in surface solar radiation in China: Evidences from current reanalyses, Journal of Geophysical Research: Atmospheres, 124, 9161-9182, https://doi.org/10.1029/2018jd030214, 2019.

Fujiwara, M., Wright, J. S., Manney, G. L., Gray, L. J., Anstey, J., Birner, T., Davis, S., Gerber,

https://doi.org/10.5194/egusphere-2026-5275
Preprint. Discussion started: 12 November 2026
© Author(s) 2026. CC BY 4.0 License.

E. P., Harvey, V. L., Hegglin, M. I., Homeyer, C. R., Knox, J. A., Krüger, K., Lambert, A., Long, C. S., Martineau, P., Molod, A., Monge-Sanz, B. M., Santee, M. L., Tegtmeier, S., Chabrillat, S., Tan, D. G. H., Jackson, D. R., Polavarapu, S., Compo, G. P., Dragani, R., Ebisuzaki, W., Harada, Y., Kobayashi, C., McCarty, W., Onogi, K., Pawson, S., Simmons, A., Wargan, K., Whitaker, J. S., and Zou, C. Z.: Introduction to the SPARC Reanalysis Intercomparison Project (S-RIP) and overview of the reanalysis systems, Atmospheric Chemistry and Physics, 17, 1417-1452, https://doi.org/10.5194/acp-17-1417-2017, 2017.

Gelaro, R., McCarty, W., Suárez, M. J., Todling, R., Molod, A., Takacs, L., Randles, C. A., Darmenov, A., Bosilovich, M. G., Reichle, R., Wargan, K., Coy, L., Cullather, R., Draper, C., Akella, S., Buchard, V., Conaty, A., da Silva, A. M., Gu, W., Kim, G.-K., Koster, R., Lucchesi, R., Merkova, D., Nielsen, J. E., Partyka, G., Pawson, S., Putman, W., Rienecker, M., Schubert, S. D., Sienkiewicz, M., and Zhao, B.: The Modern-Era Retrospective Analysis for Research and Applications, Version 2 (MERRA-2), Journal of Climate, 30, 5419-5454, https://doi.org/10.1175/JCLI-D-16-0758.1, 2017.

Guan, H., Zhu, P., Huang, J., Jin, Z., Ma, Y., Li, X., Zeng, Y., Su, W., Miao, S., Wu, W., and Wu, B.: Extreme surface solar ultraviolet radiation events reduce maize yields in China, Communications Earth & Environment, 6, 449, https://doi.org/10.1038/s43247-025-02432-9, 2025.

He, Y. and Wang, K.: Variability in direct and diffuse solar radiation across China from 1958 to 2017, Geophysical Research Letters, 47, e2019GL084570, https://doi.org/10.1029/2019gl084570, 2020.

He, Y., Wang, K., and Feng, F.: Improvement of ERA5 over ERA-Interim in simulating surface incident solar radiation throughout China, Journal of Climate, 34, 3853–3867, https://doi.org/0.1175/JCLI-D-20-0300.1, 2021a.

He, Y., Wang, K., and Qi, D.: Roles of anthropogenic forcing and natural variability in the record-breaking low sunshine event in January–February 2019 over the Middle-Lower Yangtze Plain, Bulletin of the American Meteorological Society, 102, S75-S81, https://doi.org/10.1175/BAMS-D-20-0185.1, 2021b.

He, Y., Wang, K., Zhou, C., and Wild, M.: A revisit of global dimming and brightening based on the sunshine duration, Geophysical Research Letters, 45, 4281-4289, https://doi.org/10.1029/2018gl077424, 2018.

He, Y., Wang, K., Yang, K., Zhou, C., Shao, C., and Yin, C.: Homogenized daily sunshine duration over China from 1961 to 2022, Earth System Science Data, 17, 1595-1611, https://doi.org/10.5194/essd-17-1595-2025, 2025.

He, Y., Yang, K., Ren, Y., Zou, M., Yuan, X., and Tang, W.: Causes of the Extremely Low Solar Radiation in the 2021 Growing Season over Southeastern Tibetan Plateau and Its Impact on Vegetation Growth, Bulletin of the American Meteorological Society, 104, E359-E366, https://doi.org/10.1175/bams-d-22-0122.1, 2023.

https://doi.org/10.5194/egusphere-2026-5275
Preprint. Discussion started: 12 November 2026
© Author(s) 2026. CC BY 4.0 License.

He, Y., Yang, K., Wild, M., Wang, K., Tong, D., Shao, C., and Zhou, T.: Constrained future brightening of solar radiation and its implication for China's solar power, National Science Review, 10, nwac242, https://doi.org/10.1093/nsr/nwac242, 2022.

He, Y., Yang, K., Zhang, M., Zhou, J., Li, C., Zhang, X., Tan, X., and Wang, K.: How extremes in surface incident solar radiation shape its long-term trends in China and Europe, Environmental Research Letters, 21, 034030, https://doi.org/10.1088/1748-9326/ae4112, 2026.

Hersbach, H. and Dee, D. P.: ERA5 reanalysis is in production., ECMWF Newsletter, 147, 2016.

Hersbach, H., Bell, B., Berrisford, P., Horányi, A., Sabater, M. J., Nicolas, J., Radu, R., Schepers, D., Simmons, A., Soci, C., and Dee, D.: Global reanalysis: goodbye ERA-Interim, hello ERA5, ECMWF Newsletter, 159, 17-24, https://doi.org/10.21957/vf291hehd7, 2019.

Hersbach, H., Bell, B., Berrisford, P., Biavati, G., Horányi, A., Muñoz Sabater, J., Nicolas, J., Peubey, C., Radu, R., Rozum, I., Schepers, D., Simmons, A., Soci, C., Dee, D., and Thépaut, J.-N.: ERA5 hourly data on single levels from 1940 to present Copernicus Climate Change Service (C3S) Climate Data Store (CDS) [dataset], https://doi.org/10.24381/cds.adbb2d47, 2023.

Hersbach, H., Bell, B., Berrisford, P., Hirahara, S., Horányi, A., Muñoz-Sabater, J., Nicolas, J., Peubey, C., Radu, R., Schepers, D., Simmons, A., Soci, C., Abdalla, S., Abellan, X., Balsamo, G., Bechtold, P., Biavati, G., Bidlot, J., Bonavita, M., De Chiara, G., Dahlgren, P., Dee, D., Diamantakis, M., Dragani, R., Flemming, J., Forbes, R., Fuentes, M., Geer, A., Haimberger, L., Healy, S., Hogan, R. J., Hólm, E., Janisková, M., Keeley, S., Laloyaux, P., Lopez, P., Lupu, C., Radnoti, G., de Rosnay, P., Rozum, I., Vamborg, F., Villaume, S., and Thépaut, J.-N.: The ERA5 global reanalysis, Quarterly Journal of the Royal Meteorological Society, 146, 1999-2049, https://doi.org/10.1002/qj.3803, 2020.

Hess, M., Koepke, P., and Schult, I.: Optical properties of aerosols and clouds: The software package OPAC, Bulletin of the American Meteorological Society, 79, 831-844, https://doi.org/10.1175/1520-0477(1998)079<0831:Opoaac>2.0.Co;2, 1998.

Hofstra, N., Haylock, M., New, M., and Jones, P. D.: Testing E-OBS European high-resolution gridded data set of daily precipitation and surface temperature, Journal of Geophysical Research: Atmospheres, 114, D21101, https://doi.org/10.1029/2009JD011799, 2009.

Horton, R. M., Mankin, J. S., Lesk, C., Coffel, E., and Raymond, C.: A Review of Recent Advances in Research on Extreme Heat Events, Current Climate Change Reports, 2, 242-259, https://doi.org/10.1007/s40641-016-0042-x, 2016.

Huang, J., Rikus, L. J., Qin, Y., and Katzfey, J.: Assessing model performance of daily solar irradiance forecasts over Australia, Solar Energy, 176, 615-626, https://doi.org/10.1016/j.solener.2018.10.080, 2018.

Jiang, H., Lu, N., Yao, L., Qin, J., and Liu, T.: Impact of climate changes on the stability of

https://doi.org/10.5194/egusphere-2026-5275
Preprint. Discussion started: 12 November 2026
© Author(s) 2026. CC BY 4.0 License.

706 solar energy: Evidence from observations and reanalysis, Renewable Energy, 208, 726-736,
707 https://doi.org/10.1016/j.renene.2023.03.114, 2023.

708 Kobayashi, S., Ota, Y., Harada, Y., Ebita, A., Moriya, M., Onoda, H., Onogi, K., Kamahori, H.,
709 Kobayashi, C., Endo, H., Miyaoka, K., and Takahashi, K.: The JRA-55 reanalysis: General
710 specifications and basic characteristics, Journal of the Meteorological Society of Japan, 93, 5-
711 48, https://doi.org/10.2151/jmsj.2015-001, 2015.

712 Li, D., Belitz, M., Campbell, L., and Guralnick, R.: Extreme weather events have strong but
713 different impacts on plant and insect phenology, Nature Climate Change, 15, 321-328,
714 https://doi.org/10.1038/s41558-025-02248-7, 2025.

715 Lin, S., Wang, H., Bai, W., Gao, C., and Ge, Q.: Heatwaves exacerbate the effects of early-
716 season drought on peak vegetation growth in the Northern Hemisphere, Global and Planetary
717 Change, 256, 105139, https://doi.org/10.1016/j.gloplacha.2025.105139, 2026.

718 Manara, V., Brunetti, M., Celozzi, A., Maugeri, M., Sanchez-Lorenzo, A., and Wild, M.:
719 Detection of dimming/brightening in Italy from homogenized all-sky and clear-sky surface
720 solar radiation records and underlying causes (1959–2013), Atmospheric Chemistry and
721 Physics, 16, 11145-11161, https://doi.org/10.5194/acp-16-11145-2016, 2016.

722 Mauritsen, T., Tsushima, Y., Meyssignac, B., Loeb, N. G., Hakuba, M., Pilewskie, P., Cole, J.,
723 Suzuki, K., Ackerman, T. P., Allan, R. P., Andrews, T., Bender, F. A.-M., Bloch-Johnson, J.,
724 Bodas-Salcedo, A., Brookshaw, A., Ceppi, P., Clerbaux, N., Dessler, A. E., Donohoe, A.,
725 Dufresne, J.-L., Eyring, V., Findell, K. L., Gettelman, A., Gristey, J. J., Hawkins, E., Heimbach,
726 P., Hewitt, H. T., Jeevanjee, N., Jones, C., Kang, S. M., Kato, S., Kay, J. E., Klein, S. A., Knutti,
727 R., Kramer, R., Lee, J.-Y., McCoy, D. T., Medeiros, B., Megner, L., Modak, A., Ogura, T.,
728 Palmer, M. D., Paynter, D., Quaas, J., Ramanathan, V., Ringer, M., von Schuckmann, K.,
729 Sherwood, S., Stevens, B., Tan, I., Tselioudis, G., Sutton, R., Voigt, A., Watanabe, M., Webb,
730 M. J., Wild, M., and Zelinka, M. D.: Earth's Energy Imbalance More Than Doubled in Recent
731 Decades, AGU Advances, 6, e2024AV001636, https://doi.org/10.1029/2024AV001636, 2025.

732 McPeters, R., Bhartia, P. K., Krueger, A., Herman, J., Wellemeyer, C., Seftor, C., Jaross, G.,
733 Torres, O., Moy, L., Labow, G., Byerly, W., Taylor, S., Swissler, T., and Cebula, R.: Earth Probe
734 Total Ozone Mapping Spectrometer (TOMS) Data Product User's Guide, National Aeronautics
735 and Space Administration, Goddard Space Flight Center, Greenbelt, MD, NASA Technical
736 Publication, 1998.

737 McPeters, R. D., Bhartia, P. K., Krueger, A. J., Herman, J. R., Schlesinger, B. M., Wellemeyer,
738 C. G., Seftor, C. J., Jaross, G., Taylor, S. L., Swissler, T., Torres, O., Labow, G., Byerly, W.,
739 and Cebula, R. P.: Nimbus-7 Total Ozone Mapping Spectrometer (TOMS) Data Products User's
740 Guide, National Aeronautics and Space Administration, Washington, DC, NASA Reference
741 Publication, 1996.

742 Qian, Y., Kaiser, D. P., Leung, L. R., and Xu, M.: More frequent cloud-free sky and less surface
743 solar radiation in China from 1955 to 2000, Geophysical Research Letters, 33, L01812,

https://doi.org/10.5194/egusphere-2026-5275
Preprint. Discussion started: 12 November 2026
© Author(s) 2026. CC BY 4.0 License.

https://doi.org/10.1029/2005gl024586, 2006.

Qian, Y., Wang, W., Leung, L. R., and Kaiser, D. P.: Variability of solar radiation under cloud-free skies in China: The role of aerosols, Geophysical Research Letters, 34, L12804, https://doi.org/10.1029/2006GL028800, 2007.

Qin, W., Wang, L., Zhang, M., Feng, L., Fang, H., Cai, H., Zhong, Y., Zhu, Q., and Yang, C.: A high-qualaity hourly, daily and monthly solar irradiance dataset in China during 1981-2014 based on MERRA-2 Reanalysis products, Earth System Science Data Discussions, 2019, 1-28, https://doi.org/10.5194/essd-2019-204, 2019.

Ramanathan, V., Cess, R. D., Harrison, E. F., Minnis, P., Barkstrom, B. R., Ahmad, E., and Hartmann, D.: Cloud-Radiative Forcing and Climate: Results from the Earth Radiation Budget Experiment, Science, 243, 57-63, https://doi.org/10.1126/science.243.4887.57, 1989.

Rienecker, M. M., Suarez, M. J., Gelaro, R., Todling, R., Bacmeister, J., Liu, E., Bosilovich, M. G., Schubert, S. D., Takacs, L., Kim, G.-K., Bloom, S., Chen, J., Collins, D., Conaty, A., da Silva, A., Gu, W., Joiner, J., Koster, R. D., Lucchesi, R., Molod, A., Owens, T., Pawson, S., Pegion, P., Redder, C. R., Reichle, R., Robertson, F. R., Ruddick, A. G., Sienkiewicz, M., and Woollen, J.: MERRA: NASA's Modern-Era Retrospective Analysis for Research and Applications, Journal of Climate, 24, 3624-3648, https://doi.org/10.1175/JCLI-D-11-00015.1, 2011.

Saha, S., Moorthi, S., Pan, H.-L., Wu, X., Wang, J., Nadiga, S., Tripp, P., Kistler, R., Woollen, J., Behringer, D., Liu, H., Stokes, D., Grumbine, R., Gayno, G., Wang, J., Hou, Y.-T., Chuang, H.-y., Juang, H.-M. H., Sela, J., Iredell, M., Treadon, R., Kleist, D., Van Delst, P., Keyser, D., Derber, J., Ek, M., Meng, J., Wei, H., Yang, R., Lord, S., van den Dool, H., Kumar, A., Wang, W., Long, C., Chelliah, M., Xue, Y., Huang, B., Schemm, J.-K., Ebisuzaki, W., Lin, R., Xie, P., Chen, M., Zhou, S., Higgins, W., Zou, C.-Z., Liu, Q., Chen, Y., Han, Y., Cucurull, L., Reynolds, R. W., Rutledge, G., and Goldberg, M.: The NCEP Climate Forecast System Reanalysis, Bulletin of the American Meteorological Society, 91, 1015-1058, https://doi.org/10.1175/2010BAMS3001.1, 2010.

Sanchez-Lorenzo, A., Calbó, J., Brunetti, M., and Deser, C.: Dimming/brightening over the Iberian Peninsula: Trends in sunshine duration and cloud cover and their relations with atmospheric circulation, Journal of Geophysical Research: Atmospheres, 114, https://doi.org/10.1029/2008JD011394, 2009.

Sanchez-Lorenzo, A., Wild, M., Brunetti, M., Guijarro, J. A., Hakuba, M. Z., Calbó, J., Mystakidis, S., and Bartok, B.: Reassessment and update of long-term trends in downward surface shortwave radiation over Europe (1939-2012), Journal of Geophysical Research: Atmospheres, 120, 9555-9569, https://doi.org/10.1002/2015jd023321, 2015.

Shao, C., Yang, K., Tang, W., He, Y., Jiang, Y., Lu, H., Fu, H., and Zheng, J.: Convolutional neural network-based homogenization for constructing a long-term global surface solar radiation dataset, Renewable and Sustainable Energy Reviews, 169, 112952,

https://doi.org/10.5194/egusphere-2026-5275
Preprint. Discussion started: 12 November 2026
© Author(s) 2026. CC BY 4.0 License.

https://doi.org/10.1016/j.rser.2022.112952, 2022.

Stephens, G. L.: Cloud Feedbacks in the Climate System: A Critical Review, Journal of Climate, 18, 237-273, https://doi.org/10.1175/JCLI-3243.1, 2005.

Takahashi, C., Shiogama, H., Imada, Y., Kosaka, Y., Mori, M., Arai, M., Kamae, Y., and Watanabe, M.: The effects of natural variability and climate change on the record low sunshine over Japan during August 2017, Bulletin of the American Meteorological Society, 100, S67-S71, https://doi.org/10.1175/bams-d-18-0107.1, 2019.

Tang, W. J., Yang, K., Qin, J., Cheng, C. C. K., and He, J.: Solar radiation trend across China in recent decades: a revisit with quality-controlled data, Atmospheric Chemistry and Physics, 11, 393-406, https://doi.org/10.5194/acp-11-393-2011, 2011.

Teng, X., Xu, L., Zhang, F., Cheng, Y., Gao, M., Chen, X., Li, J., Zhou, S., Shu, S., Zhu, S., Liu, D., Zhao, C., Ching, J., and Li, W.: Low Cloud Dispersion Effects by Anthropogenic Aerosols in Polluted Air, Geophysical Research Letters, 53, e2025GL120887, https://doi.org/10.1029/2025GL120887, 2026.

Tong, D., Farnham, D. J., Duan, L., Zhang, Q., Lewis, N. S., Caldeira, K., and Davis, S. J.: Geophysical constraints on the reliability of solar and wind power worldwide, Nature Communications, 12, 6146, https://doi.org/10.1038/s41467-021-26355-z, 2021.

Urraca, R., Huld, T., Gracia-Amillo, A., Javier Martinez-de-Pison, F., Kaspar, F., and Sanz-Garcia, A.: Evaluation of global horizontal irradiance estimates from ERA5 and COSMO-REA6 reanalyses using ground and satellite-based data, Solar Energy, 164, 339-354, https://doi.org/10.1016/j.solener.2018.02.059, 2018.

Wang, A. H. and Zeng, X. B.: Evaluation of multireanalysis products with in situ observations over the Tibetan Plateau, Journal of Geophysical Research-Atmospheres, 117, D05102, https://doi.org/10.1029/2011jd016553, 2012.

Wang, K., Ma, Q., Li, Z., and Wang, J.: Decadal variability of surface incident solar radiation over China: observations, satellite retrievals, and reanalyses, Journal of Geophysical Researc: Atmospheres, 120, 6500-6514, https://doi.org/10.1002/2015jd023420, 2015.

Wang, L., Liu, Y., Zhao, L., Lu, X., Huang, L., Jin, Y., Davis, S. J., Aghakouchak, A., Huang, X., Zhu, T., and Qin, Y.: Unraveling climate change-induced compound low-solar-low-wind extremes in China, National Science Review, 12, nwae424, https://doi.org/10.1093/nsr/nwae424, 2024.

Wang, X. L. and Feng, Y.: RHtestsV4 user manual. Environment Canada Science and Technology Directorate Climate Research. [Available online at http://etccdi.pacificclimate.org/software.shtml.], 2013.

Wang, X. L. L.: Penalized maximal F test for detecting undocumented mean shift without trend change, Journal of Atmospheric and Oceanic Technology, 25, 368-384,

https://doi.org/10.5194/egusphere-2026-5275
Preprint. Discussion started: 12 November 2026
© Author(s) 2026. CC BY 4.0 License.

https://doi.org/10.1175/2007jtecha982.1, 2008.

Wang, X. L. L., Chen, H. F., Wu, Y. H., Feng, Y., and Pu, Q. A.: New Techniques for the Detection and Adjustment of Shifts in Daily Precipitation Data Series, Journal of Applied Meteorology and Climatology, 49, 2416-2436, https://doi.org/10.1175/2010jamc2376.1, 2010.

Wang, Y. and Wild, M.: A new look at solar dimming and brightening in China, Geophysical Research Letters, 43, 11777-11785, https://doi.org/10.1002/2016gl071009, 2016.

Wild, M.: Global dimming and brightening: A review, Journal of Geophysical Research: Atmospheres, 114, D00D16, https://doi.org/10.1029/2008jd011470, 2009.

Wild, M.: Enlightening global dimming and brightening, Bulletin of the American Meteorological Society, 93, 27-37, https://doi.org/10.1175/bams-d-11-00074.1, 2012.

Wild, M., Wang, Y., Wang, K., and Yang, S.: A Perspective on Global Dimming and Brightening Worldwide and in China, Advances in Atmospheric Sciences, 43, 281-294, https://doi.org/10.1007/s00376-025-4534-2, 2026.

Wilks, D. S.: Statistical methods in the atmospheric sciences, Academic press2011.

Wohland, J., Brayshaw, D., Bloomfield, H., and Wild, M.: European multidecadal solar variability badly captured in all centennial reanalyses except CERA20C, Environmental Research Letters, 15, 104021, https://doi.org/10.1088/1748-9326/aba7e6, 2020.

Yang, K., Huang, G. W., and Tamai, N.: A hybrid model for estimating global solar radiation, Solar Energy, 70, 13-22, https://doi.org/10.1016/s0038-092x(00)00121-3, 2001.

Yang, K., Koike, T., and Ye, B.: Improving estimation of hourly, daily, and monthly solar radiation by importing global data sets, Agricultural and Forest Meteorology, 137, 43-55, https://doi.org/10.1016/j.agrformet.2006.02.001, 2006.

Yang, S., Wang, X. L., and Wild, M.: Homogenization and trend analysis of the 1958-2016 in situ surface solar radiation records in China, Journal of Climate, 31, 4529-4541, https://doi.org/10.1175/jcli-d-17-0891.1, 2018.

Yuan, T., Song, H., Kramer, R., Oreopoulos, L., Raghuraman, S. P., Wood, R., and Chin, M.: Aerosol effective radiative forcing increases Earth's energy imbalance in recent decades, Nature Communications, Online Press, https://doi.org/10.1038/s41467-026-72926-3, 2026.

Zhao, C. F., Yang, Y. K., Fan, H., Huang, J. P., Fu, Y. F., Zhang, X. Y., Kang, S. C., Cong, Z. Y., Letu, H., and Menenti, M.: Aerosol characteristics and impacts on weather and climate over the Tibetan Plateau, National Science Review, 7, 492-495, https://doi.org/10.1093/nsr/nwz184, 2020.

Zheng, D., Tong, D., Davis, S. J., Qin, Y., Liu, Y., Xu, R., Yang, J., Yan, X., Geng, G., Che, H., and Zhang, Q.: Climate change impacts on the extreme power shortage events of wind-solar

https://doi.org/10.5194/egusphere-2026-5275
Preprint. Discussion started: 12 November 2026
© Author(s) 2026. CC BY 4.0 License.



852 supply systems worldwide during 1980–2022, Nature Communications, 15, 5225,
853 https://doi.org/10.1038/s41467-024-48966-y, 2024.

854 Zhou, C., He, Y., and Wang, K.: On the suitability of current atmospheric reanalyses for
855 regional warming studies over China, Atmospheric Chemistry and Physics, 18, 8113-8136,
856 https://doi.org/10.5194/acp-18-8113-2018, 2018.

857 Zhou, C., Wang, K., and Ma, Q.: Evaluation of eight current reanalyses in simulating land
858 surface temperature from 1979 to 2003 in China, Journal of Climate, 30, 7379-7398,
859 https://doi.org/10.1175/jcli-d-16-0903.1, 2017.

860 Zhou, C., Wang, J., Dai, A., and Thorne, P.: A New Approach to Homogenize Global Subdaily
861 Radiosonde Temperature Data from 1958 to 2018, Journal of Climate, 34, 1163-1183,
862 https://doi.org/10.1175/jcli-d-20-0352.1, 2021.

863

https://doi.org/10.5194/egusphere-2026-5275
Preprint. Discussion started: 12 November 2026
© Author(s) 2026. CC BY 4.0 License.

Table 1 Trends in the frequency (units: days·decade^{-1}) and magnitude (units: W·m^{-2}·decade^{-1}) of extremely low (R_s10p) and high (R_s90p) surface incident solar radiations from observations (OBS), ERA5, and MERRA-2 in China during 1961–1979, 1980–1993, and 1994–2016 periods. Bold and italic denote significance at the 0.05 and 0.10 levels, respectively.

		OBS	ERA5	MERRA-2
R_s90p frequency	1961–1979	**-18.31**	-0.97	
	1980–1993	*-5.00*	-5.27	-6.01
	1994–2016	**6.65**	0.60	**-6.44**
R_s90p magnitude	1961–1979	-0.26	*-4.78*	
	1980–1993	**13.35**	2.76	7.12
	1994–2016	1.52	2.26	-0.85
R_s10p frequency	1961–1979	1.89	-1.15	
	1980–1993	**2.79**	**5.26**	0.84
	1994–2016	**1.92**	-0.84	**2.43**
R_s10p magnitude	1961–1979	-0.07	0.56	
	1980–1993	**-3.70**	**-4.18**	**-5.26**
	1994–2016	**1.37**	-0.58	**1.67**

https://doi.org/10.5194/egusphere-2026-5275
Preprint. Discussion started: 12 November 2026
© Author(s) 2026. CC BY 4.0 License.

Figure Captions

Figure 1 Spatial distribution of the 55 solar radiation stations across China with homogeneous observations for 1961–2016. Star symbols denote the locations of the stations, with their colors representing the percentage of valid daily observations during 1961–2016. Background color shading represents elevation (m).

Figure 2 (a) Annual mean anomalies of surface incident solar radiation (R_s; unit: $W \cdot m^{-2}$) from observations (gray), ERA5 (solid dark orange), and MERRA-2 (dashed light orange) over China during 1961–2016 and (b–i) their spatial patterns of trends (unit: $W \cdot m^{-2} \cdot decade^{-1}$) during three periods: (b–c) 1961–1979, (d–f) 1980–1993, and (g–i) 1994–2016. Black-bordered dots indicate significance at a level of 0.10, whereas light gray-bordered dots indicate statistically insignificant results. The proportions of positive ($p < 0.10$; red bar) and negative ($p < 0.10$; blue bar) R_s trends are shown in each panel.

Figure 3 Thresholds of surface incident solar radiation (R_s; unit: $W \cdot m^{-2}$) corresponding to different quantiles (10%, 30%, 50%, 70%, and 90%) of for each calendar day based on observations (OBS, thick solid), ERA5 (thin solid), and MERRA-2 (thin dashed) over their respective analysis periods.

Figure 4 Climatology of frequency and magnitude of extremely high surface incident solar radiations (R_s90p) across China averaged over three periods: (a–b) 1961–1979, (c–e) 1980–1993, and (f–h) 1994–2016. Dot size indicates the magnitude (unit: $W \cdot m^{-2}$), while dot color denotes the frequency (unit: days).

Figure 5 Same as Figure 4, but for extremely low surface incident solar radiation (R_s10p).

Figure 6 Performance of reanalysis products in capturing extremely (a) high (R_s90p) and (b)

https://doi.org/10.5194/egusphere-2026-5275
Preprint. Discussion started: 12 November 2026
© Author(s) 2026. CC BY 4.0 License.

low (R_s10p) surface incident solar radiation based on several metrics including accuracy, precision, specificity, false-alarm rate, hit rate, and miss rate, for ERA5 (dark orange) and MERRA-2 (light orange) evaluated against observations during 1980–2016.

Figure 7 Time series of (a–b) frequency (unit: days) and (c–d) magnitude (unit: $W \cdot m^{-2}$) in extremely high (R_s90p) and low (R_s10p) surface incident solar radiations in China from 1961 to 2016, based on observations (gray), ERA5 (solid dark orange), and MERRA-2 (dashed light orange).

Figure 8 Trend maps of frequency and magnitude of extremely high (R_s90p) surface incident solar radiations from observations (OBS), ERA5 and MERRA-2 in China during three periods: (a–b) 1961–1979, (c–e) 1980–1993, and (f–h) 1994–2016. Colors indicate trends in R_s90p frequency (unit: $days \cdot decade^{-1}$) with black dots marking significance at a level of 0.1. Upward and downward triangles denote increasing and decreasing trends in R_s90p magnitude (unit: $W \cdot m^{-2} \cdot decade^{-1}$), respectively, with their sizes indicating the absolute trend magnitudes. Black and light gray triangle outlines indicate statistically significant ($p < 0.10$) and insignificant ($p > 0.10$) trends, respectively. The pie chart in the lower-left corner of each panel shows the proportions of stations exhibiting different combinations of frequency and magnitude trends: (+/+) indicates increasing trends in both, (+/-) indicates an increasing frequency but decreasing magnitude, (-/-) indicates decreasing trends in both, and (-/+) indicates a decreasing frequency but increasing magnitude. Due to integer rounding, the sum of percentages for each pie chart may not equal exactly 100% of the theoretical total.

https://doi.org/10.5194/egusphere-2026-5275
Preprint. Discussion started: 12 November 2026
© Author(s) 2026. CC BY 4.0 License.

Figure 9 Same as Figure 8, but for extremely low surface incident solar radiation (R_s10p).

Figure 10 Scatterplots of multi-year mean biases in extremely low (R_s10p; blue dots) and high (R_s90p; red dots) surface incident solar radiations (R_s; unit: W·m^{-2}) versus biases in (a–b) total cloud cover (TCC; unit: %) and (c–d) clear-sky surface incident solar radiation (R_c; unit: W·m^{-2}) during 1980–2013 at the 55 stations. The starting year of 1980 was selected based on the temporal overlap of ERA5 and MERRA-2 from 1980 onwards, whereas 2013 marks the end-year since the data availability of cloud cover ends in 2013. The biases are computed as reanalyses minus observations for extreme R_s days identified separately within each dataset. "*r*" denotes correlation coefficient with a statistical significance level in parentheses and "slope" indicates linear regression slope. Each dot denotes the reanalysis bias at an individual station, thus their correlation coefficients across the stations reflect the spatial correlations of the biases.

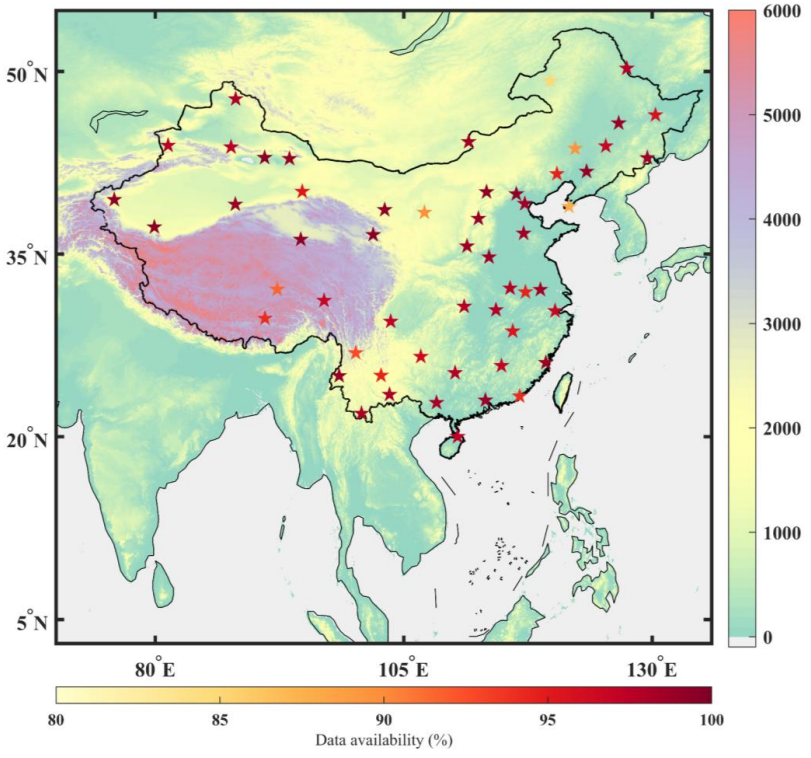
Figure 11 Same as Figure 10, but the biases are computed as reanalyses minus observations for extreme R_s days identified based on observations.

Figure 12 (a–h) Maps of partial correlation coefficients (ρ) derived from annual bias time series between reanalysis biases in extreme surface incident solar radiations (i.e., R_s10p and R_s90p) and their physical drivers (i.e., total cloud cover, TCC, and clear-sky R_s, R_c) during 1980–2013 across 55 stations. Black and light gray outlines indicate statistically significant ($p < 0.05$) and insignificant ($p > 0.05$) levels, respectively. The biases were computed as reanalyses minus observations for extreme R_s days identified separately within each dataset. (i) Violin plots summarizing the station-level ρ shown in (a–h).

https://doi.org/10.5194/egusphere-2026-5275
Preprint. Discussion started: 12 November 2026
© Author(s) 2026. CC BY 4.0 License.

Figure 13 Relative contributions (%) of trend biases in total cloud cover (ΔTCC) and clear-sky surface incident solar radiation (ΔR_c) to those in extreme surface incident solar radiations (ΔR_s10p and ΔR_s90p) from (a–d) ERA5 and (e–h) MERRA-2 relative to observations from 55 ground-based stations.

https://doi.org/10.5194/egusphere-2026-5275
Preprint. Discussion started: 12 November 2026
© Author(s) 2026. CC BY 4.0 License.



935

936 **Figure 1** Spatial distribution of the 55 solar radiation stations across China with homogeneous
937 observations for 1961–2016. Star symbols denote the locations of the stations, with their colors
938 representing the percentage of valid daily observations during 1961–2016. Background color
939 shading represents elevation (m).

https://doi.org/10.5194/egusphere-2026-5275
Preprint. Discussion started: 12 November 2026
© Author(s) 2026. CC BY 4.0 License.

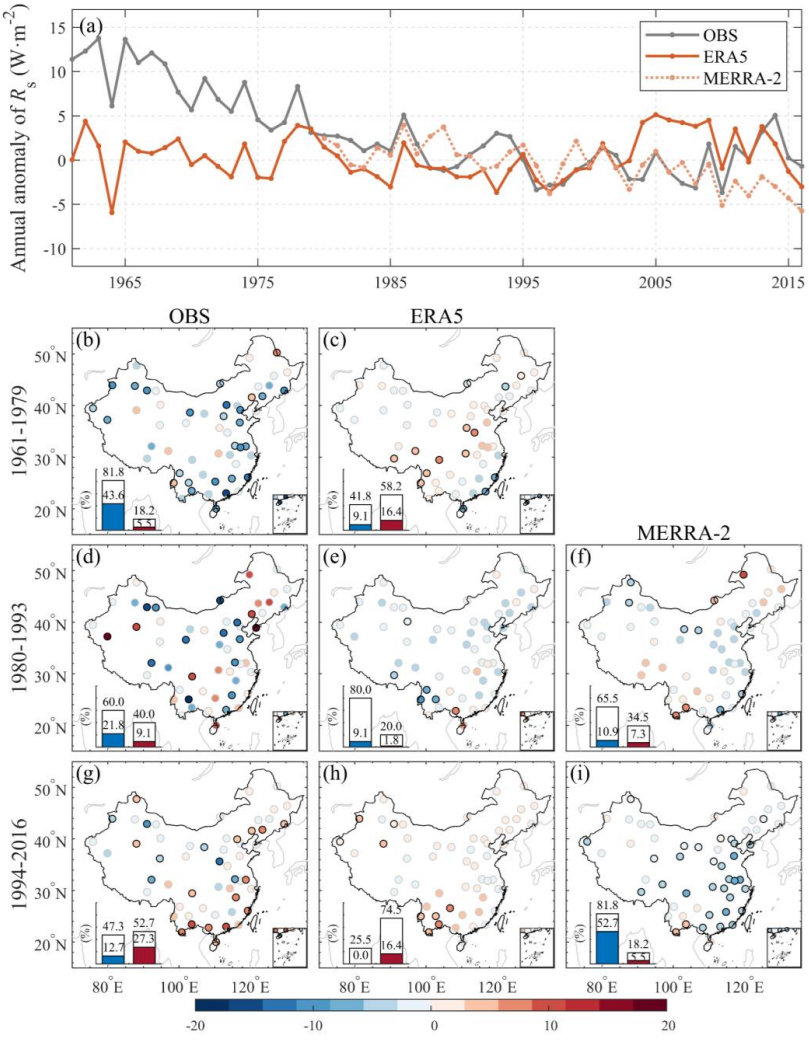
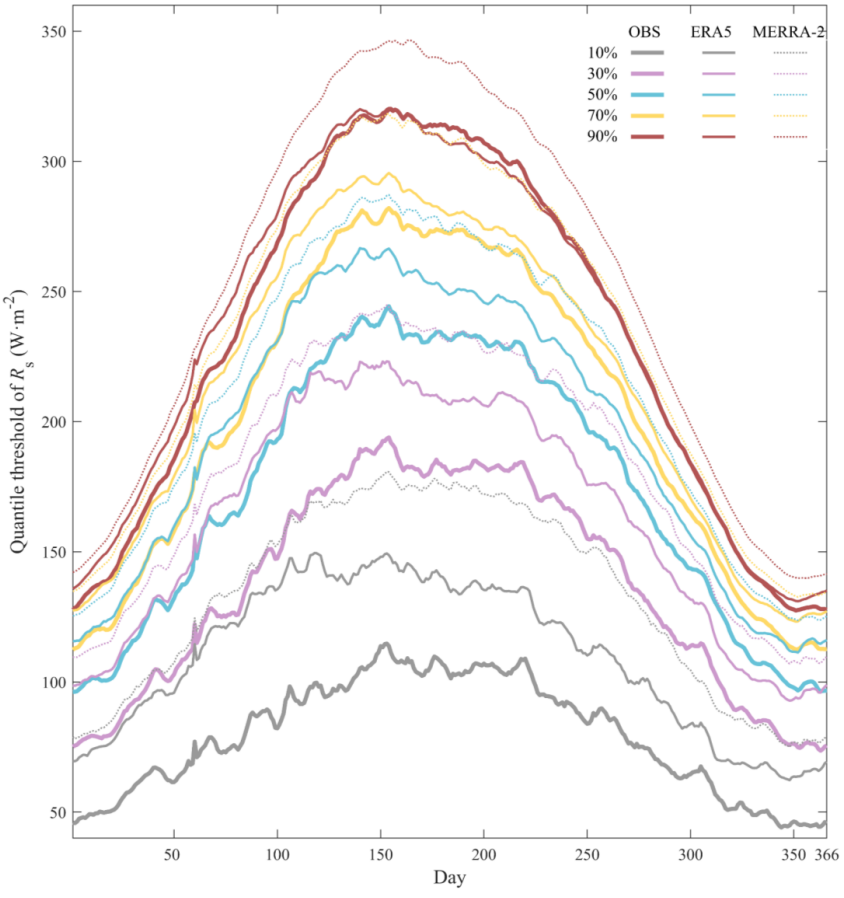


Figure 2 (a) Annual mean anomalies of surface incident solar radiation (R_s; unit: W·m^{-2}) from observations (gray), ERA5 (solid dark orange), and MERRA-2 (dashed light orange) over China during 1961–2016 and (b–i) their spatial patterns of trends (unit: W·m^{-2}·decade^{-1}) during three periods: (b–c) 1961–1979, (d–f) 1980–1993, and (g–i) 1994–2016. Black-bordered dots indicate significance at a level of 0.10, whereas light gray-bordered dots indicate statistically insignificant results. The proportions of positive (p < 0.10; red bar) and negative (p < 0.10; blue bar) R_s trends are shown in each panel.

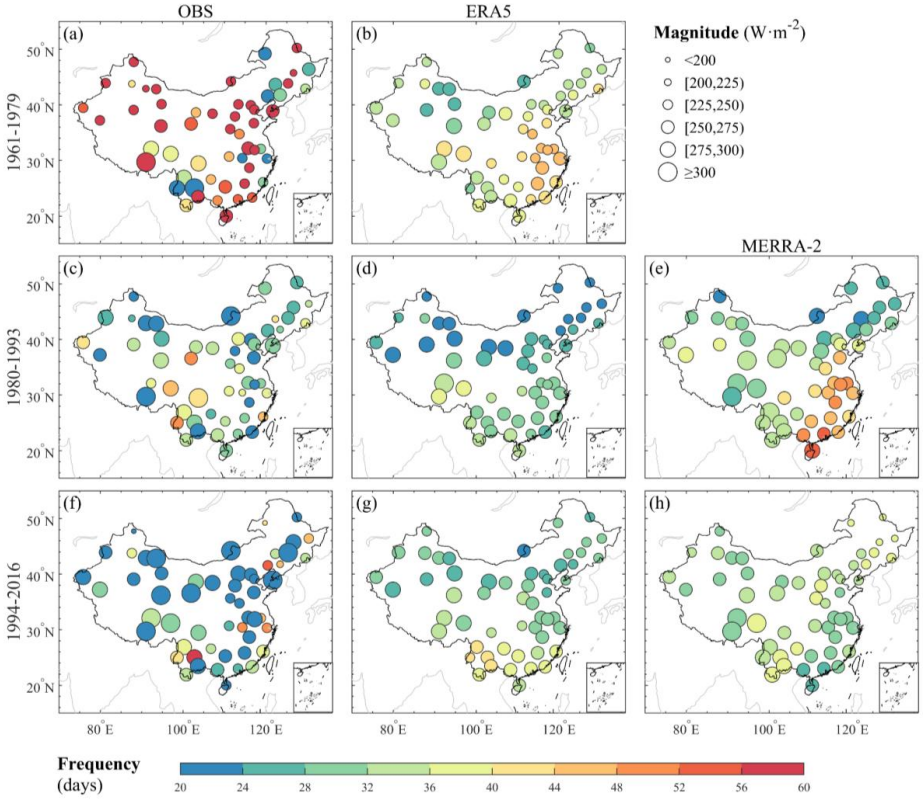
https://doi.org/10.5194/egusphere-2026-5275
Preprint. Discussion started: 12 November 2026
© Author(s) 2026. CC BY 4.0 License.



948

949 **Figure 3** Thresholds of surface incident solar radiation (R_s; unit: W·m^{-2}) corresponding to
950 different quantiles (10%, 30%, 50%, 70%, and 90%) of for each calendar day based on
951 observations (OBS, thick solid), ERA5 (thin solid), and MERRA-2 (thin dashed) over their
952 respective analysis periods.

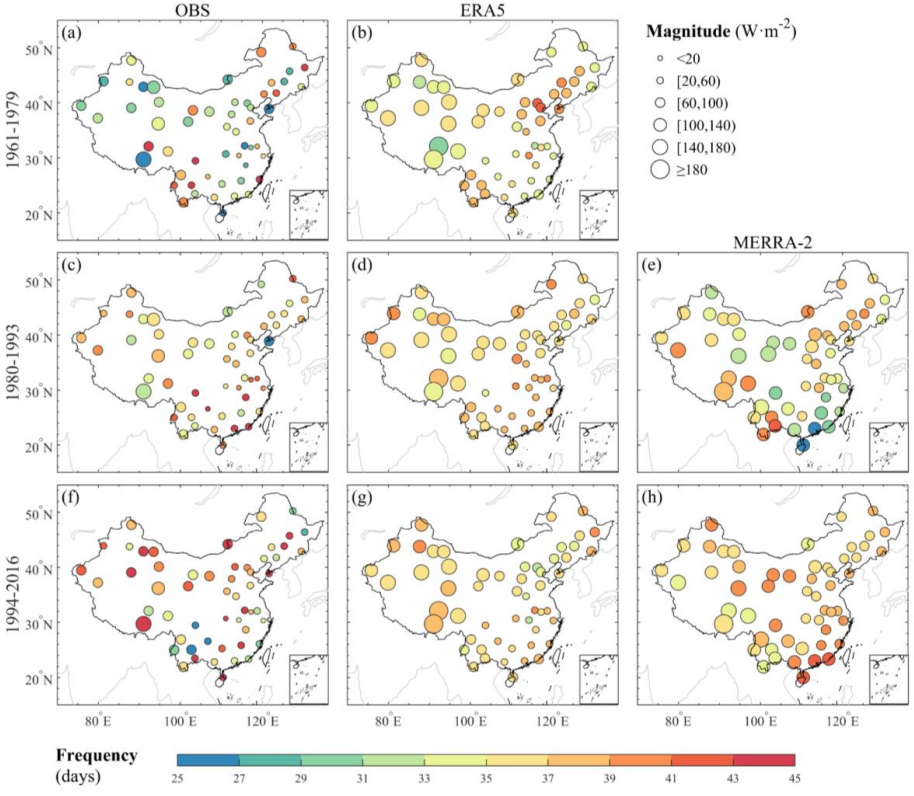
https://doi.org/10.5194/egusphere-2026-5275
Preprint. Discussion started: 12 November 2026
© Author(s) 2026. CC BY 4.0 License.



953

954 **Figure 4** Climatology of frequency and magnitude of extremely high surface incident solar
955 radiations (R_s90p) across China averaged over three periods: (a–b) 1961–1979, (c–e) 1980–
956 1993, and (f–h) 1994–2016. Dot size indicates the magnitude (unit: W·m^{-2}), while dot color
957 denotes the frequency (unit: days).

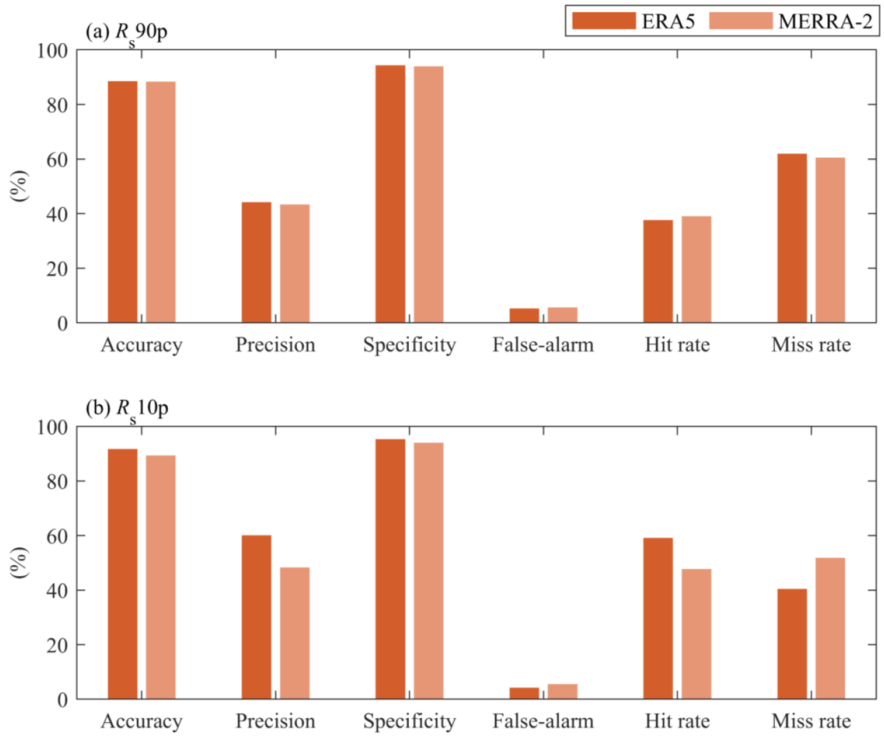
https://doi.org/10.5194/egusphere-2026-5275
Preprint. Discussion started: 12 November 2026
© Author(s) 2026. CC BY 4.0 License.



958

959 **Figure 5** Same as Figure 4, but for extremely low surface incident solar radiation (R_s10p).

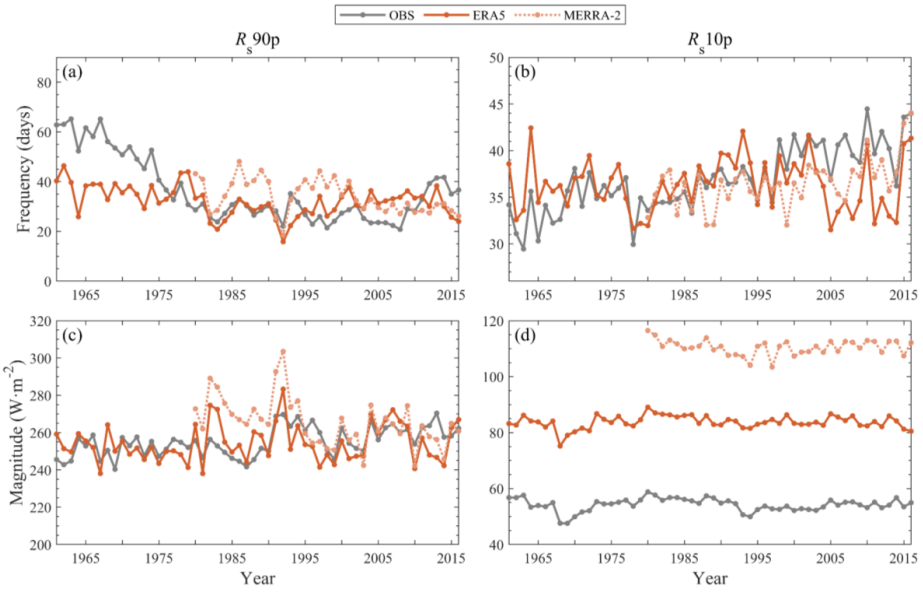
https://doi.org/10.5194/egusphere-2026-5275
Preprint. Discussion started: 12 November 2026
© Author(s) 2026. CC BY 4.0 License.



960

961 **Figure 6** Performance of reanalysis products in capturing extremely (a) high (R_s90p) and (b)
962 low (R_s10p) surface incident solar radiation based on several metrics including accuracy,
963 precision, specificity, false-alarm rate, hit rate, and miss rate, for ERA5 (dark orange) and
964 MERRA-2 (light orange) evaluated against observations during 1980–2016.

https://doi.org/10.5194/egusphere-2026-5275
Preprint. Discussion started: 12 November 2026
© Author(s) 2026. CC BY 4.0 License.



965

966 **Figure 7** Time series of (a–b) frequency (unit: days) and (c–d) magnitude (unit: W·m^{-2}) in
967 extremely high (R_s90p) and low (R_s10p) surface incident solar radiations in China from 1961
968 to 2016, based on observations (gray), ERA5 (solid dark orange), and MERRA-2 (dashed light
969 orange).

https://doi.org/10.5194/egusphere-2026-5275
Preprint. Discussion started: 12 November 2026
© Author(s) 2026. CC BY 4.0 License.

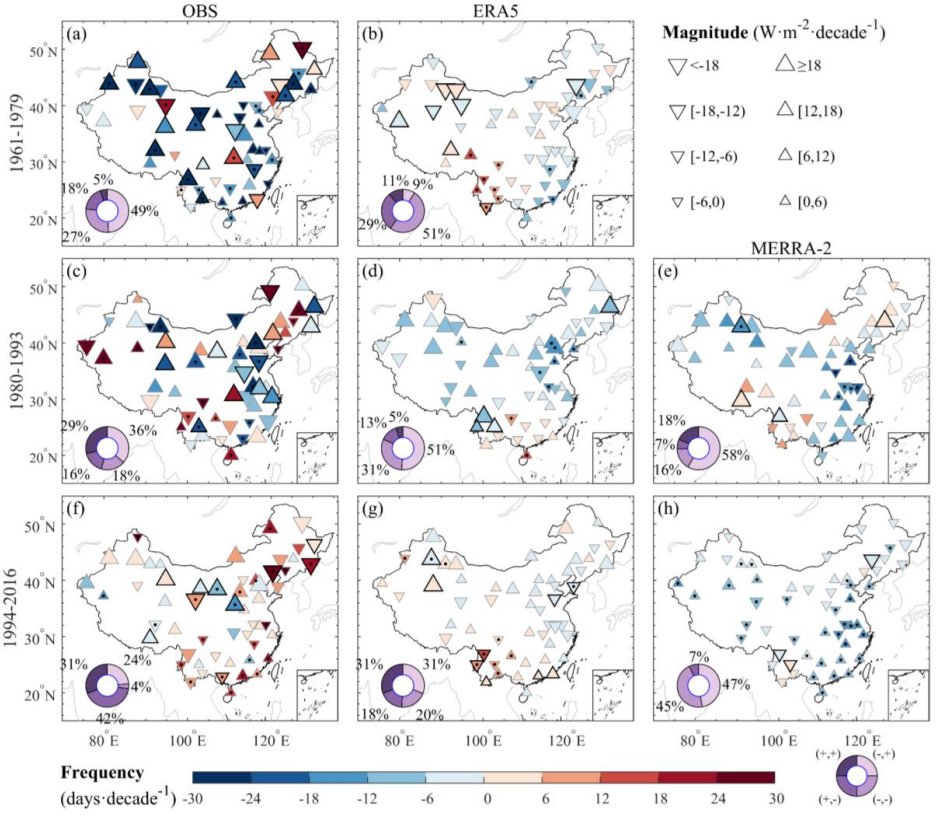
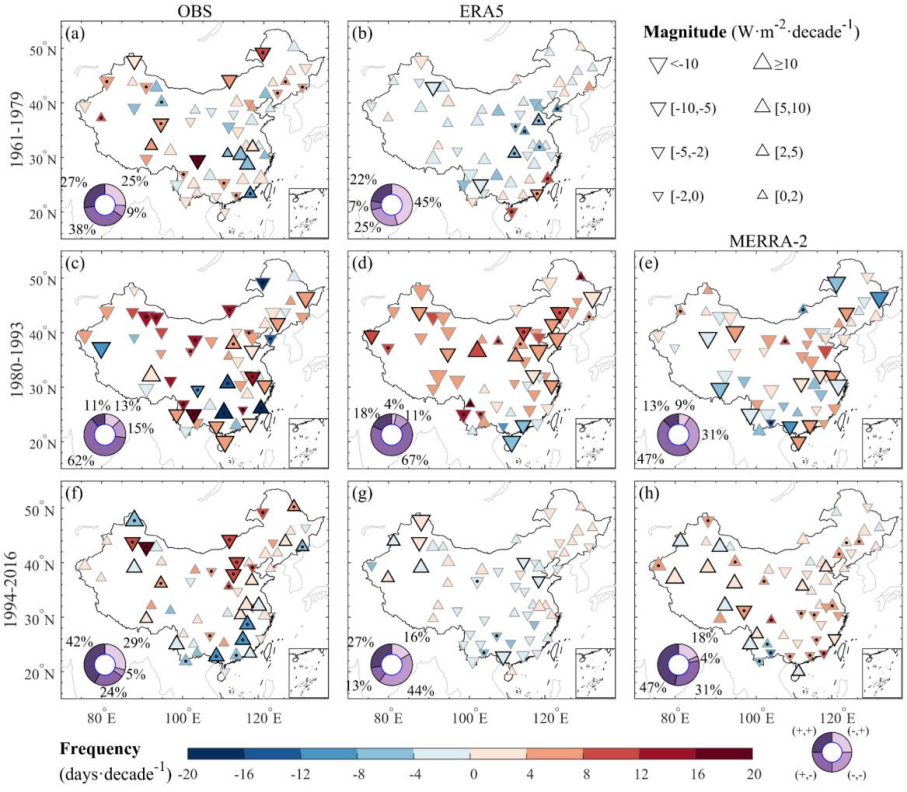


Figure 8 Trend maps of frequency and magnitude of extremely high (R_s90p) surface incident solar radiations from observations (OBS), ERA5 and MERRA-2 in China during three periods: (a–b) 1961–1979, (c–e) 1980–1993, and (f–h) 1994–2016. Colors indicate trends in R_s90p frequency (unit: days·decade^{-1}) with black dots marking significance at a level of 0.10. Upward and downward triangles denote increasing and decreasing trends in R_s90p magnitude (unit: W·m^{-2}·decade^{-1}), respectively, with their sizes indicating the absolute trend magnitudes. Black and light gray triangle outlines indicate statistically significant ($p < 0.10$) and insignificant ($p > 0.10$) trends, respectively. The pie chart in the lower-left corner of each panel shows the proportions of stations exhibiting different combinations of frequency and magnitude trends: (+/+) indicates increasing trends in both, (+/-) indicates an increasing frequency but decreasing

https://doi.org/10.5194/egusphere-2026-5275
Preprint. Discussion started: 12 November 2026
© Author(s) 2026. CC BY 4.0 License.

magnitude, (-/-) indicates decreasing trends in both, and (-/+) indicates a decreasing frequency but increasing magnitude. Due to integer rounding, the sum of percentages for each pie chart may not equal exactly 100% of the theoretical total.

https://doi.org/10.5194/egusphere-2026-5275
Preprint. Discussion started: 12 November 2026
© Author(s) 2026. CC BY 4.0 License.



984

985 **Figure 9** Same as Figure 8, but for extremely low surface incident solar radiation (R_s10p).

https://doi.org/10.5194/egusphere-2026-5275
Preprint. Discussion started: 12 November 2026
© Author(s) 2026. CC BY 4.0 License.

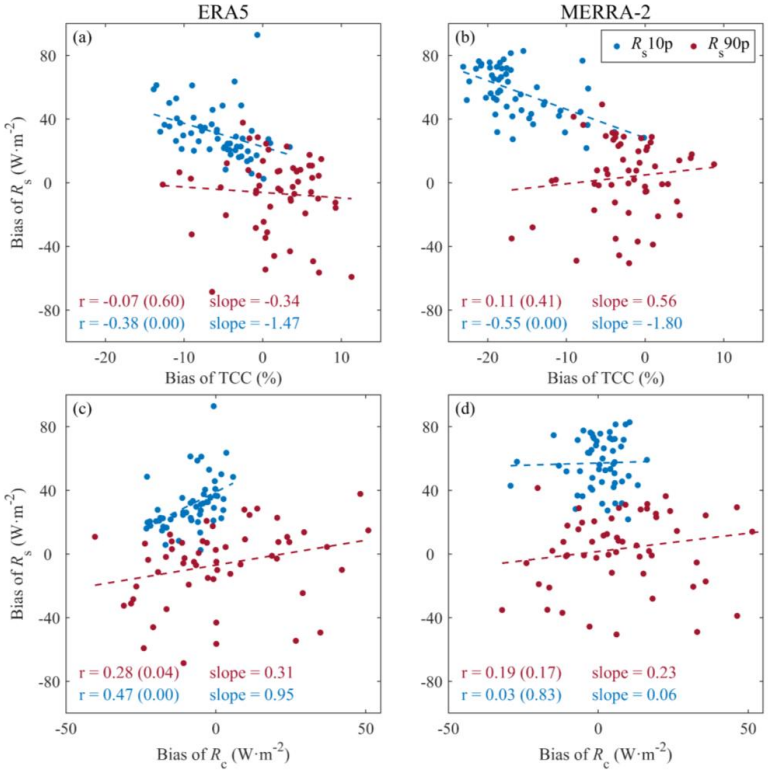
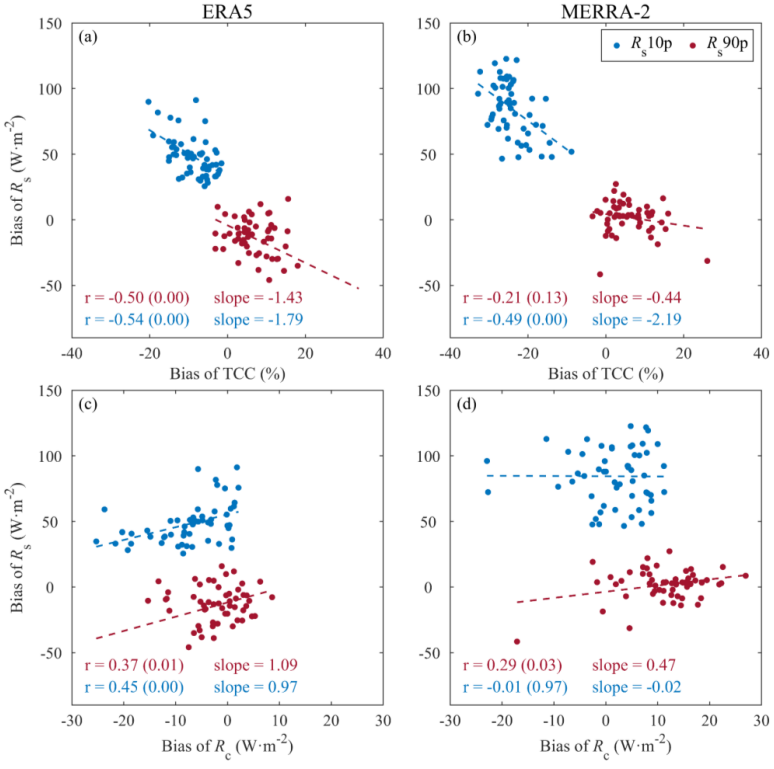


Figure 10 Scatterplots of multi-year mean biases in extremely low (R_s10p; blue dots) and high (R_s90p; red dots) surface incident solar radiations (R_s; unit: W·m^{-2}) versus biases in (a–b) total cloud cover (TCC; unit: %) and (c–d) clear-sky surface incident solar radiation (R_c; unit: W·m^{-2}) during 1980–2013 at the 55 stations. The starting year of 1980 was selected based on the temporal overlap of ERA5 and MERRA-2 from 1980 onwards, whereas 2013 marks the end-year since the data availability of cloud cover ends in 2013. The biases were computed as reanalyses minus observations for extreme R_s days identified separately within each dataset. "*r*" denotes correlation coefficient with a statistical significance level in parentheses and "slope" indicates linear regression slope. Each dot denotes the reanalysis bias at an individual station, thus their correlation coefficients across the stations reflect the spatial correlations of the biases.

https://doi.org/10.5194/egusphere-2026-5275
Preprint. Discussion started: 12 November 2026
© Author(s) 2026. CC BY 4.0 License.



997

998 **Figure 11** Same as Figure 10, but the biases are computed as reanalyses minus observations

999 for extreme R_s days identified based on observations.

https://doi.org/10.5194/egusphere-2026-5275
Preprint. Discussion started: 12 November 2026
© Author(s) 2026. CC BY 4.0 License.

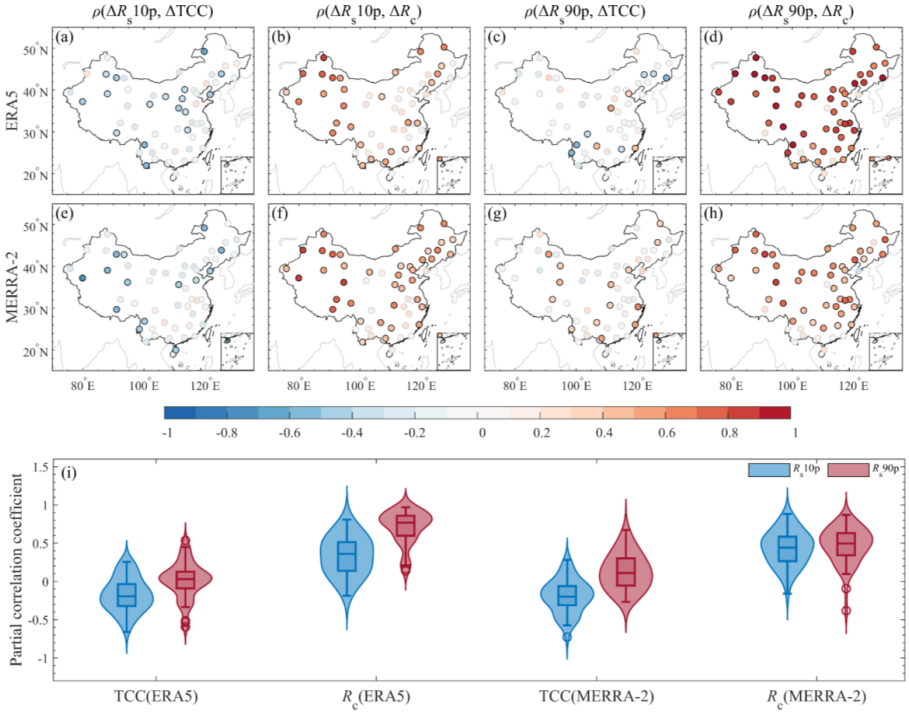


Figure 12 (a–h) Maps of partial correlation coefficients (ρ) derived from annual bias time series between reanalysis biases in extreme surface incident solar radiations (i.e., R_s10p and R_s90p) and their physical drivers (i.e., total cloud cover, TCC, and clear-sky R_s, R_c) during 1980–2013 across 55 stations. Black and light gray outlines indicate statistically significant ($p < 0.05$) and insignificant ($p > 0.05$) levels, respectively. The biases were computed as reanalyses minus observations for extreme R_s days identified separately within each dataset. (i) Violin plots summarizing the station-level ρ shown in (a–h).

https://doi.org/10.5194/egusphere-2026-5275
Preprint. Discussion started: 12 November 2026
© Author(s) 2026. CC BY 4.0 License.

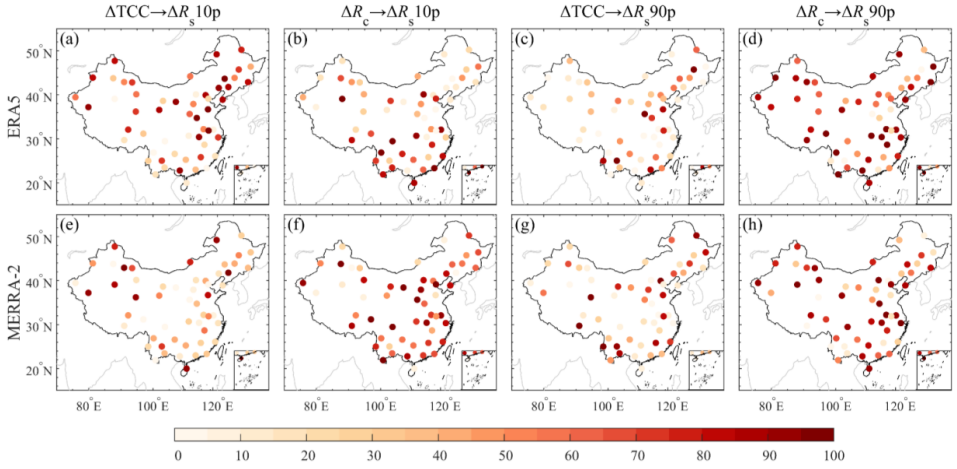


Figure 13 Relative contributions (%) of trend biases in total cloud cover (ΔTCC) and clear-sky surface incident solar radiation (ΔR_c) to those in extremely low and high surface incident solar radiations (ΔR_s10p and ΔR_s90p) in (a–d) ERA5 and (e–h) MERRA-2 relative to observations at 55 ground-based stations.